Engineering Structures 233 (2021) 111944

Contents lists available at ScienceDirect

Engineering Structures

journal homepage: www.elsevier.com/locate/engstruct

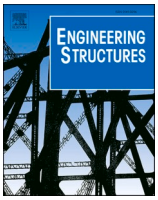

Probabilistic prediction model for RC bond failure mode

Ahmad Soraghi [a,*], Qindan Huang [b]

[a] Department of Civil Engineering, University of Akron, ASEC 210, Sumner St, Akron, OH 44325, USA
[b] Department of Civil, Construction, and Environmental Engineering, Marquette University, 1637 W. Wisconsin Ave, Milwaukee, WI 53233, USA

ARTICLE INFO

Keywords:
Reinforced concrete
Bond
Corrosion
Probabilistic models
Failure mode
Classification methods
Reliability

ABSTRACT

Adequate rebar-concrete bonding is crucial to ensure the reliable performance of reinforced concrete (RC) structures. Many factors such as the concrete properties, concrete cover depth, transverse reinforcement, and the presence of corrosion will affect the bond behavior, and consequently, the structural performance. While many prior studies have focused on the influence of the aforementioned factors on the bond strength, the impact of these factors on the bond failure mode has not been thoroughly investigated. A probabilistic bond failure mode prediction model that considers various influencing factors including loading type and corrosion is developed in this study. This study uses the bond testing results of 132 beam-end specimens subjected to monotonic and cyclic loading and adopts classification methods to develop the prediction model, which is then used to evaluate the impact of bond behavior on the reliability of a RC beam with a lap splice.

1. Introduction

Reinforced concrete (RC) is a widely used construction material for civil structures like bridges [1,2], buildings [3], and dams [4]. As the bond between rebar and concrete (i.e., rebar–concrete interaction) is meant to ensure the transformation of force between the rebar and concrete, bond behavior directly impacts the structure load-carrying capacity and failure mode. This bond is known to be influenced by many factors such as the concrete properties, transverse reinforcement, the ratio of concrete cover to rebar size, loading type, and rebar corrosion. Many researchers have studied how those influencing factors affect the bond strength, through which impact structural performance [5–13].

Another aspect of bond behavior that is also crucial for determining the performance of RC structures is the bond failure mode. Based on ACI [14], there are two distinguished bond failure mode: pull-out and splitting failure. Pull-out bond failure occurs when there is sufficient confinement and/or concrete cover to prevent concrete splitting and restrain crack growth, resulting in the shearing of concrete between ribs. Splitting failure occurs when confinement or cover is not provided adequately to achieve the complete pull-out strength. In splitting failure, the deformation-bearing forces cause splitting that spreads through the sides of the member and makes the concrete to lose its bonding and cover.

In contrast to bond strength, the bond failure mode has not been well studied, especially in the presence of corrosion and/or under cyclic loading. Both ACI [14] criteria and CEB [15] use bar size, concrete cover, and confinement of transverse stirrups to determine the bond failure mode. Cucchiara et al. [16] and Zandi Hanjari et al. [17] examined the impact of the existence of the stirrups on the failure mode. Kivell [5] observed that specimens with high levels of corrosion (more than 12%) or under cyclic loading have more tendency to fail in pull-out. Soraghi and Huang [7] developed models for predicting the bond failure mode using logistic and lasso classification algorithms to consider various influence factors including the presence of transverse stirrups, cover to rebar diameter ratio, the level of corrosion, and the loading type.

This study develops probabilistic prediction models of bond failure mode based on classification methods and examines the importance of bond failure mode prediction in the structure performance evaluation. The model development uses the results from a comprehensive experimental testing where various influencing factors are considered, including compressive strength of concrete, ratio of concrete cover to rebar diameter ratio, confinement of transverse stirrups, corrosion level, and loading type.

In this paper, the bond tests conducted on a set of beam-end specimens are described first, next the probabilistic models based on various classification methods are developed, and then the prediction accuracy of the models is compared. Lastly, a case study is presented using the developed bond failure mode prediction model to examine how the

* Corresponding author.
E-mail addresses: as481@uakron.edu (A. Soraghi), qindan.huang@marquette.edu (Q. Huang).

https://doi.org/10.1016/j.engstruct.2021.111944
Received 11 August 2020; Received in revised form 16 January 2021; Accepted 22 January 2021
Available online 5 February 2021

Table 1
Summary of design parameters of testing specimens.

Group	f'_c (MPa)		No. of specimens (Imperial rebar size)			No. of specimens (Loading type*)		No. of intact specimens	Corroded specimens w/ corrosion, Q (%)		c/d	K_{tr}
	Target	Actual							Target	Actual		
1	25	27	16 (#5)	16 (#6)	12 (#8)	18 (M)	26 (C)	12	5–20	3.2–15.6	1.3–4.8	0 or 3.6–5.8
2	35	36	16 (#5)	16 (#6)	12 (#8)	22 (M)	22 (C)	6	5–15	4.93–19.0		7.3–11.7
3	45	43	16 (#5)	16 (#6)	12 (#8)	22 (M)	22 (C)	6	5–15	3.74–16.8		7.3–11.7

* (M) Monotonic, and (C) cyclic.

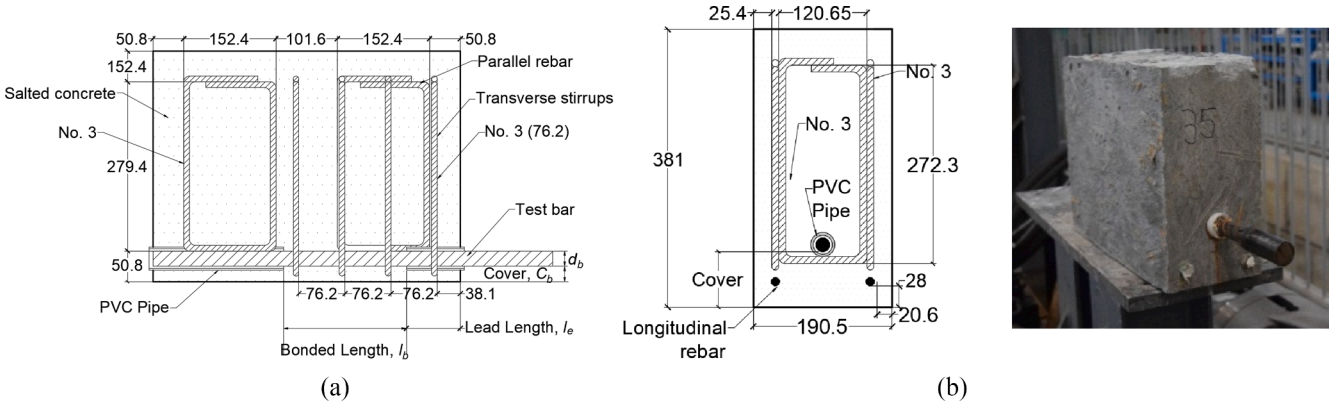

Fig. 1. Beam-end specimens: (a) schematic design and (b) as-casted beam-end specimen.

bond impacts the flexural performance of an RC beam with a lap splice under various corrosion levels based on the reliability analysis.

2. Experimental program

2.1. Specimen design and details

A set of beam-end specimens are designed to investigate the intact and corroded rebar bond behavior under monotonic and cyclic loading. The design of the specimens are based on four parameters that found to be influencing bond behavior according to the findings of previous studies (e.g., [7,13,18,19]) and they are: concrete compressive strength (f'_c), cover size to rebar diameter ratio (c/d), corrosion level (Q), and transverse rebar confinement that can be quantified by an index value, K_{tr} [20], as shown below:

$$K_{tr} = \frac{f_{y,tr} \cdot A_{tr}}{4136.85 \cdot d_b \cdot s} \quad (1)$$

where $f_{y,tr}$ is the yield strength of transverse reinforcement (kN/m^2), A_{tr} is the transverse reinforcement area (m^2), d_b is the diameter of intact rebar (m), and s is the spacing of the transverse reinforcement (m). The detailed specification for each specimen is provided in Tables A1–A3 in Appendix A. Table 1 summarizes the ranges of the design parameters. The specimens are classified into three groups (as shown in Table 1) based on the three designated concrete compressive strength levels: 25 MPa, 35 MPa, and 45 MPa (corresponding to measured averages of 27 MPa, 36 MPa, and 43 MPa, respectively, obtained in the cylinder tests). Each of the three groups consists of 44 beam-end specimens; thus, 132 specimens are tested. The level of corrosion, Q, is the percentage of mass reduction of the reinforcement in the bonded region. Group 1 consists of 22 corroded specimens with the designed Q ranging from 5% to 20% (corresponding to measured Q of 3.2% to 15.6% after load testing was completed) and 12 intact specimens (Q = 0%). Group 2 consists of 38 corroded specimens with the designed Q ranging from 5% to 15% (corresponding to measured Q of 4.93% to 19.08% after testing was completed) and 6 intact specimens. Group 3 also consists of 38 corroded specimens with designed Q ranging from 5% to 15% (corresponding to measured Q of 3.74% to 16.85% after load testing was completed) and 6 intact specimens.

Specimens in each group use three sizes of reinforcement bars: #5 bars (d_b = 15.875 mm), #6 bars (d_b = 19.05 mm), and #8 bars (d_b = 25.4 mm). Among the 44 specimens in Group 1, 22 have transverse stirrups with K_{tr} values ranging from 3.68 to 5.89, and the remaining 22 specimens have no transverse stirrups (i.e., K_{tr} = 0). All specimens in Groups 2 and 3 have transverse stirrups to increase the chance of pull-out failure, with K_{tr} values ranging from 7.3 to 11.7. For loading type, in Group 1, 18 of the specimens are tested under monotonic loading, while 26 specimens are tested under cyclic loading; in groups 2 and 3, 22 specimens in each group have monotonic loading and the other 22 specimens have cyclic loading.

Dimensions and reinforcement detailing for the designed beam-end specimens are shown in Fig. 1(a), and Fig. 1(b) shows an actual casted beam-end specimen. All specimens are 508 mm × 381 mm × 190.5 mm. All transverse, parallel, and longitudinal reinforcements are #3 rebar with a diameter of 76.2 mm. All the reinforcements are coated with epoxy to prevent corrosion except for the test bar. The test bar is covered by PVC pipes at the two ends within the concrete. The middle bonded region of the test bar that is not covered by PVC pipe has a bonded length, l_b, as shown in Fig. 1(a), and l_b = 88.9 mm, 114.3 mm, and 152.4 mm are adopted for the specimens with rebar sizes of #5, #6, and #8, respectively. These bonded lengths are chosen to prevent rebar tensile yielding prior to bond failure, to ensure a relatively uniform distribution of bond stress [13], and prevent conical failure of the specimens [21]. The yield strength, F_y, and ultimate strength, F_u, of rebar are 420 MPa and 600 MPa, respectively, regardless of the rebar size.

To accelerate corrosion on the test bar, sodium chloride (NaCl) was added to the concrete before it was poured into the specimen molds. The amount of salt (NaCl) in the concrete is calculated based on 3.75% weight of cement as is suggested by previous researchers [22,23] to achieve accelerated corrosion.

2.2. Corrosion process

Accelerated corrosion is achieved by applying current to the test bar.

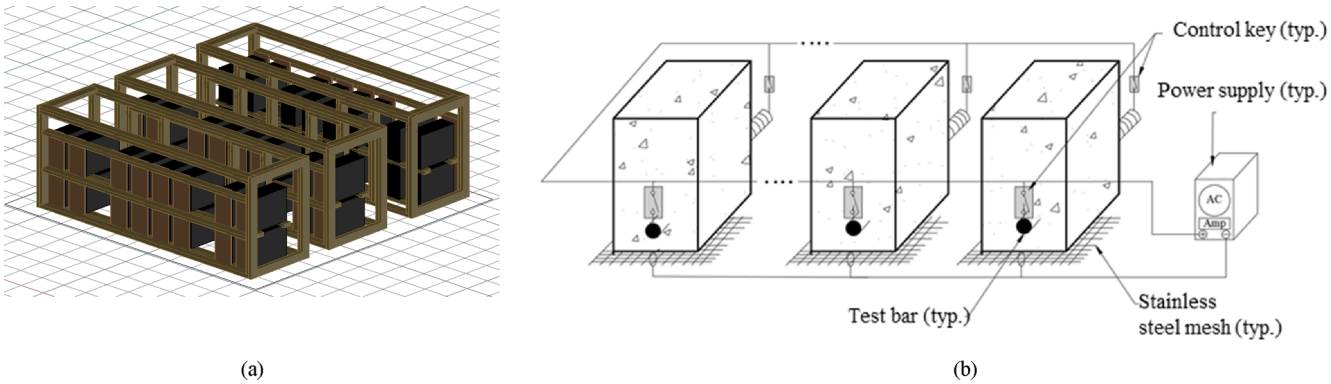

Fig. 2. Schematic view of (a) humidity tents and (b) corrosion setup.

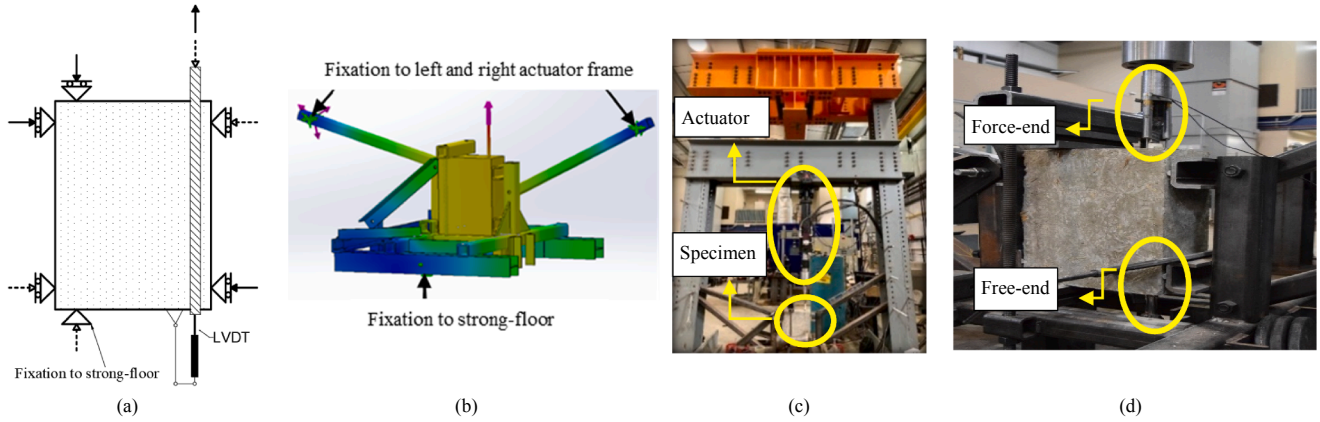

Fig. 3. (a) Boundary conditions of testing specimen; (b) 3D rendering view of test setup; (c) testing frame, (d) laboratory test setup.

The designed corrosion level can be calculated as:

$$Q = \frac{\Delta M}{\gamma \cdot l_b \cdot A_{b0}} \times 100\% \tag{2}$$

where ΔM (grams) is the change in mass of the rebar due to corrosion; $\gamma = 7.86$ gr/cm^3 is the density of iron, l_b is the corroded length (or bond length), and A_{b0} refers to the intact cross-sectional area of rebar. With a desired level of Q, ΔM can be estimated based on Eq. (2). Then the accelerated corrosion time, T, during which the current needs to be applied can be calculated to achieve the desired corrosion level based on Faraday's law [24]:

$$T = \frac{\Delta M \cdot Z \cdot F}{A \cdot I} \tag{3}$$

where $A = 56$ g referring to the atomic weight of iron; I is current (Amp); $Z = 2$ is the valency number of ions of the substance, Fe, and $F = 96500$ (Amp·sec), which is referred to as Faraday's constant.

After casting, the specimens are cured with sufficient humidity [25]. In this study, all specimens are kept in the designed humidity tents (schematically shown in Fig. 2(a)) for curing as well as corroding. The corrosion setup (schematically shown in Fig. 2(b)) is designed to allow power supplies to be connected to the specimens to supply the required current for accelerating corrosion while keeping the specimens in the humidity tents. The corrosion setup uses a parallel circuit system where the rebar serves as the anode, while a stainless steel plate that was located underneath the specimen (mostly underneath the bonded region) acts as the cathode [26]. The parallel system allows specimen(s) to be removed without stopping the current that runs through the other specimens, and such a setup is necessary, as each specimen is designed for different corrosion levels and requires a different corrosion time. In addition, the parallel system allows the use of power supplies with lower voltage compared to a setup using a series circuit system.

2.3. Test setup

Monotonic and cyclic testing are performed to study the corrosion impact on bond behavior. Utilizing the testing frame that is securely mounted on a rigid floor in the testing lab, a vertical test setup is designed for this study based on ASTM A944-10 and a previous study by Bandelt and Billington [27] where the applied loading on beam-end specimens is in a vertical direction as well. Fig. 3(a) and 3(b) are a schematic of the setup that shows the boundary conditions and a 3D-rendering view of the setup, respectively. It should be noted that the roller/pin supports were provided at six locations, where three supports react (shown in solid arrows) when the rebar is under tension and the other three supports react (shown in dashed arrows) when the rebar is under compression, as shown in Fig. 3(a). Fig. 3(c) and (d) show the testing frame and the laboratory test setup, respectively.

A 245-kN actuator is secured to the testing frame in a vertical position; a threaded rod is welded to the test bar and the specimen connects to the actuator through a special connection designed particularly for this test. Rebar slippage is measured according to ASTM standard A944-10 [28] using linear variable differential transducers (LVDTs) at the free-end of the specimen. The LVDTs are mounted on the bottom of the concrete as shown in Fig. 3(a) such that the slippage of the rebar relative to the bottom of the concrete could be measured.

To accomplish the testing, it is necessary to first determine the loading procedure and loading rate. ASTM standard 944-10 [28] specifies that a loading rate between 10% and 33% of the predicted rupture force be reached within one minute. However, this rate is too fast to

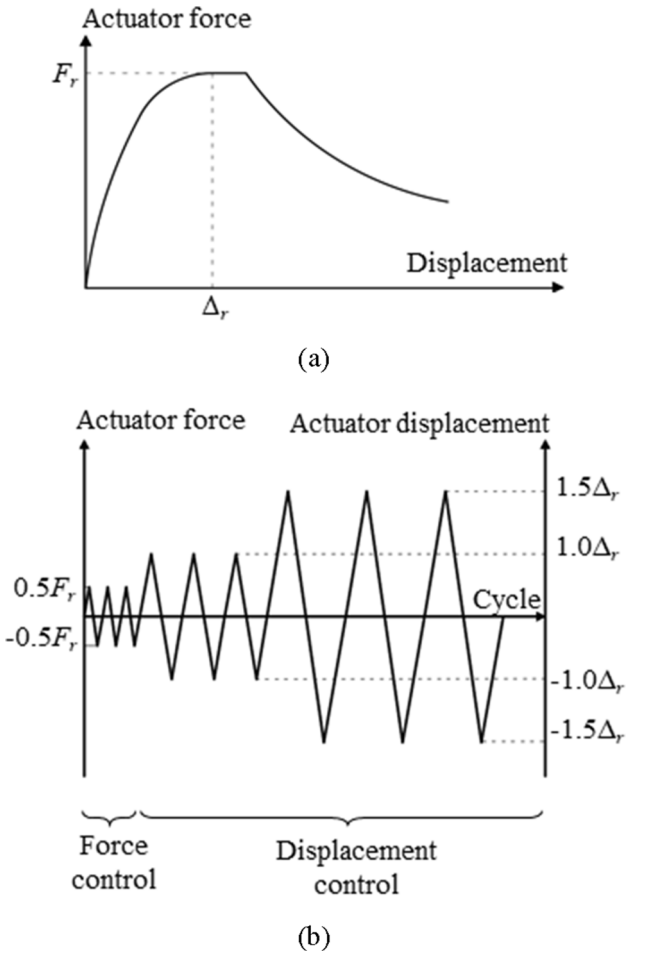

Fig. 4. (a) Actuator force and displacement diagram under monotonic loading and (b) cyclic loading protocol.

allow recording the critical points during the failure process, particularly the point at which the rupture force occurs (i.e., the bond strength is achieved). Thus, the loading rate is recalculated in such a way that the rupture force will not occur in less than three minutes. Accordingly, all monotonic specimens are tested in displacement-control with a rate equal to 0.005 mm/sec (that is, 1.3 mm per 3 min). Fig. 4(a) shows an actuator force-displacement diagram under monotonic loading, where F_r is the rupture force and Δ_r is the displacement of the actuator at rupture.

As ASTM standard 944-10 does not specify the cyclic loading procedure for bond testing, the procedure used in Kivell [5] is adopted in this study. Fig. 4(b) shows the adopted cyclic loading protocol consists of three sets of cycles, where F_r and Δ_r are extracted from the corresponding monotonic curve (Fig. 4(a)).

In the cyclic loading, the first set of cycles are force-controlled with a maximum force of $0.5F_r$; the other two sets of cycles are displacement-controlled with maximum displacements of $1.0\Delta_r$ and $1.5\Delta_r$, respectively. The first set is mainly used for weakening the bond, while the second and third sets of cycles are designed to break the bond and capture the behavior after exceeding the bond strength. For the force-controlled cycles, the loading rate is $10\%F_r \sim 33\%F_r$ per minute; for the displacement-controlled cycles, the displacement rate is $10\%\Delta_r \sim 33\%\Delta_r$ per minute.

2.4. Experimental results and discussion

After testing is complete, the monotonic and cyclic bond behaviors of all specimens are obtained. The work presented in this paper focuses on the prediction of the failure modes; the study on the other bond characteristics (e.g., bond strength) will be presented in future papers. Two distinct failure modes, pull-out and splitting failure are observed, and the failure modes for each specimen are summarized in Table A1-A3 in Appendix A, where failure mode "P" refers to the pull-out failure and "S" is the splitting failure. However, there were 12 specimens whose failure modes were not distinguishable due to various reasons (e.g., the actuator reached its force capacity before the bond failure occurred); these specimens are marked as "NA" in failure mode. Fig. 5 shows the typical actuator force-displacement diagrams under monotonic or cyclic loading with splitting or pull-out failure modes. A common feature of splitting failure under either monotonic or cyclic loading is the sudden drop in force when the specimen reaches its rupture force, followed by observing large surface and/or sides cracks on the specimen.

In addition, different crack patterns are observed for the two failure modes. Fig. 6 shows typical crack patterns for pull-out and splitting failure modes, and Fig. 7 presents a schematic view of crack patterns for each mode of failure. Generally, with splitting failure, not only the surface of the specimen is crushed, but at least one crack is initiated from the testing rebar as shown in Fig. 7(a). This is because such surface cracks are propagated from the radial splitting of the concrete due to the wedge action of the test bar ribs when the bond fails in splitting. However, with pull-out failure, the cracks do not initiate from the testing rebar (as shown in Fig. 7(b)), as there is sufficient confinement to restrain the concrete surrounding the rebar from splitting. Darwin and Graham [21] also found that splitting failure (which was the only failure mode observed in their specimens) have some crack patterns based on the presence of transverse stirrups as well as on the cover size, which is consistent with the splitting mode cracking patterns observed in this study. Thus, identifying the cracking pattern could help to determine the failure mode.

3. Probabilistic prediction model for bond failure mode

In this section, existing deterministic models for bond failure mode and various classification algorithms are reviewed. The logistic and lasso classification algorithms used in the model development are described, and the performances of the various prediction models are compared

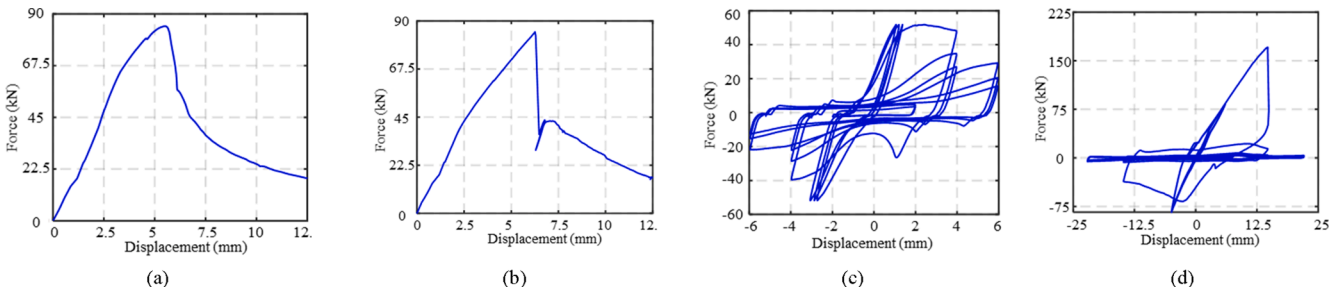

Fig. 5. Typical actuator force-displacement (a) under monotonic loading with pull-out failure, (b) under monotonic loading with splitting failure, (c) under cyclic loading with pull-out failure, and (d) under cyclic loading with splitting failure.

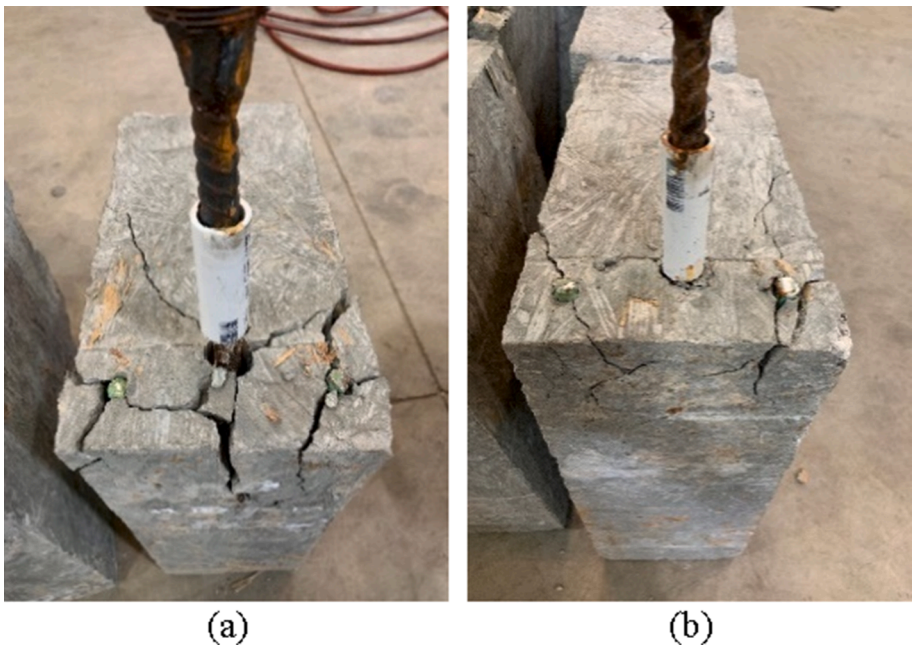

Fig. 6. A typical cracking pattern for (a) splitting failure mode and (b) pull-out failure mode.

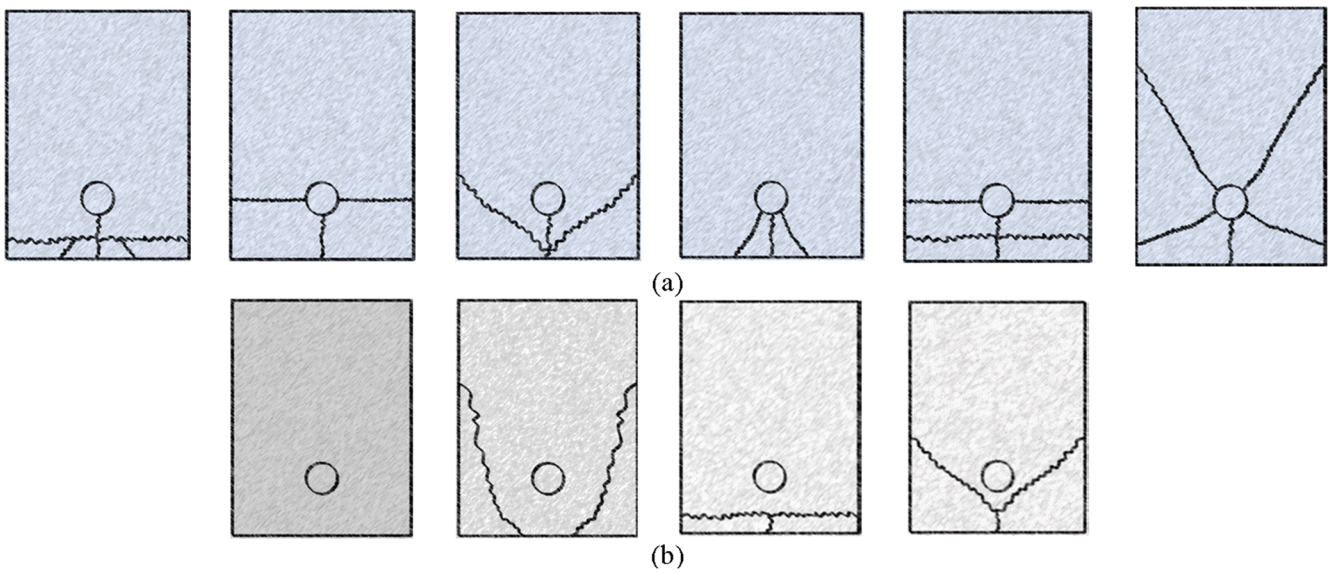

Fig. 7. Schematic view of crack patterns formed on the test specimens after failure: (a) splitting failure mode and (b) pull-out failure mode.

based on the experimental data.

3.1. Existing deterministic models

In the literature, very few models are available for predicting RC bond failure modes. If let $Y = 1$ and $Y = 0$ represent pull-out and splitting bond failure, respectively, the prediction by CEB criteria can be written as [15]:

$$Y = \begin{cases} 1 & c \geqslant 5d_b \\ 0 & c_{max}/c_{min} = 2.0 \,\&\, c_{min} = d_b \,\&\, d_b \leqslant 20\,\text{mm} \,\&\, K_{tr,CEB} = 2\% \end{cases} \quad (4a)$$

where $c_{max} = \max\{c_x, c_{si}\}$ and $c_{min} = \min\{c_x, c_y, c_{si}\}$, in which c_x and c_y are the concrete cover toward the horizontal and vertical edges, respectively, and c_{si} is the half of the center-to-center test bar spacing (if more than one test bar is implemented); $K_{tr,CEB} = A_{tr}/(n_b \cdot d_b \cdot s)$, in which nb is the number of anchored test bars. However, it is obvious that conditions for splitting failure (i.e., $c_{max}/c_{min} = 2.0$, $c_{min} = d_b$ and $K_{tr,CEB} = 2\%$) are very strict, which makes these CEB criteria almost inapplicable. Thus, instead of using the CEB criteria literally, the "equal" sign in the expressions may be interpreted to be "no larger than", and the logical operator between the expressions be interpreted to be "or", rather than "and". Also, for the cases that do not satisfy both pull-out and splitting conditions of the CEB criteria, the prediction can be treated as "unknown". Thus, the CEB criteria is interpreted as follows in this study:

$$Y = \begin{cases} 1 & c \geqslant 5d_b \\ 0 & c_{max}/c_{min} \leqslant 2.0 \text{ or } c_{min} \leqslant d_b \text{ or } d_b \leqslant 20\text{mm or } K_{tr,CEB} \leqslant 2\% \\ \text{unknown} & \text{otherwise} \end{cases} \quad (4b)$$

Meanwhile, ACI [29] uses the following criteria for the bond failure mode prediction:

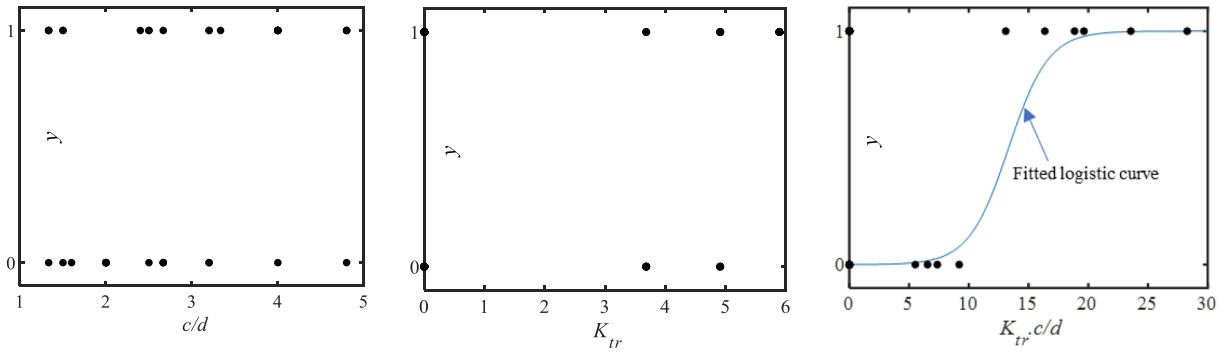

Fig. 8. Example of a scatter plot of failure mode for terms (a) c/d, (b) K_{tr}, and (c) logistic curve for their interaction term (K_{tr}·c/d).

$$Y = \begin{cases} 1 \left(c + K_{tr,\mathrm{ACI}}/d_b\right) \geqslant 2.5 \\ 0 \left(c + K_{tr,\mathrm{ACI}}/d_b\right) < 2.5 \end{cases} \tag{5}$$

where $K_{tr,\mathrm{ACI}} = A_{tr} \cdot f_{y,tr}/(1500 \cdot s \cdot n_b)$.

The two prediction models shown above are deterministic based; thus, uncertainty is not considered. More importantly, these two models do not holistically consider all the parameters that might influence the bond failure mode, such as corrosion and loading types.

3.2. Classification algorithms

Supervised machine learning techniques (i.e. regression and classification) are extensively implemented in engineering purposes for response estimation. Whilst the regression algorithm is appropriate for continuous response prediction, the classification algorithm is suitable for categorical responses such as failure modes [30]. In this study, classification methods are used to develop probabilistic models based on all the influencing parameters. In the following, a brief description of the classification algorithms of logistic and lasso classification is described, and other classification algorithms adopted in this research is provided in Appendix B.

3.2.1. Logistic classification

The logistic classification algorithm evaluates the relationship between independent variables and dependent variables (i.e., categorical response) using a logistic function. The binary response, Y, refers to the bond failure mode and is defined as the same as before: $Y = 1$ for pull-out and $Y = 0$ for splitting. The formulation for logistic classification to estimate the probability of pull-out failure is shown as:

$$Pr(Y = 1|\mathbf{x}) = \frac{exp(z)}{1 + exp(z)} = \frac{exp\left(\beta_0 + \sum_{i=1}^{m} \beta_i \mathbf{x}_i\right)}{1 + exp\left(\beta_0 + \sum_{i=1}^{m} \beta_i \mathbf{x}_i\right)} \tag{6}$$

where $\mathbf{x} = \{x_i\}$, in which x_i are the independent variables selected, m is the number of independent variables used, and β_0 and $\{\beta_i\}$ are the coefficients for logistic classification that can be obtained using the maximum likelihood technique [31] through a likelihood function as:

$$l(\boldsymbol{\beta}) = \sum_{j=1}^{N} \left(y_j \boldsymbol{\beta}^{\mathrm{T}} \widetilde{\mathbf{x}}_j - log\left[1 + exp\left(\widetilde{\mathbf{x}}_j \boldsymbol{\beta}\right)\right]\right) \tag{7}$$

where the subscript j refers to the j^{th} observation data, $\mathbf{x}_j = \{1\ \mathbf{x}\}^{\mathrm{T}}$, and $\boldsymbol{\beta} = \{\beta_0\, \beta_1\, \beta_2 \ldots \beta_m\}^{\mathrm{T}}$. As Y is a binary variable, then $P(Y = 0|\mathbf{x}) = 1 - P(Y = 1|\mathbf{x})$. It should be noted that the deviance of the fitted model is proportional to $-\log[l(\boldsymbol{\beta})]$; accordingly, by maximizing $l(\boldsymbol{\beta})$ for the $\boldsymbol{\beta}$ evaluation, the deviance will be minimized.

3.2.2. Lasso classification

While the lasso classification uses the same formulation (shown in Eq. (6)) as the logistic algorithm, the way to evaluate the model parameters is different. Lasso classification requires a constraint on the coefficients in the maximum likelihood evaluation, which can be expressed as:

$$l(\boldsymbol{\beta}) = \sum_{j=1}^{N} \left(y_j \boldsymbol{\beta}^{\mathrm{T}} \mathbf{x}_j - ln\left[1 + exp\left(\mathbf{x}_j \boldsymbol{\beta}\right)\right] - \lambda \sum_{i=0}^{p} |\beta_i|\right) \tag{8}$$

where λ is a penalty factor also known as the constraint. Lasso classification stabilizes a system by applying a cost of the sum of absolute values of the coefficients. This is called sparse regularization to constrain over-fitting and is conducted using the *lassoglm* function in MATLAB by which the deviance will be minimized in order to estimate the model parameters in Eq. (8). Lasso classification is a more desirable technique when working with a relatively small size of data, or when there is a correlation between independent variables [32], and lasso's strength is to reduce the fitted model deviance without substantially increasing the prediction bias.

3.3. Model development

From an engineering perspective, logistic and lasso classification are capable of providing explicit formulations. For this reason, both methods are used in developing the probabilistic model. Other methods, including the two deterministic models and other classification algorithms (i.e., decision tree, discriminant analysis, K-nearest neighbors, Naïve-Bayes, random forest, and support vector machine) that are described in Appendix B, will be assessed in terms of their model prediction accuracy.

3.3.1. Independent variables selected for the models

To develop the failure mode prediction models based on Eq. (6), a preliminary analysis needs to be performed first to select the potential variable x_i [33]. Next, a model selection procedure is used to delete the independent variables that are not contributing significantly to the model prediction.

In this study, the variables showing the potential impacts on the failure mode (Y) are: f'_c, c/d, K_{tr}, Q, and MC, where MC is a dummy variable defined as:

$$MC = \begin{cases} 1 & \text{monotonic loading} \\ 2 & \text{cyclic loading} \end{cases} \tag{9}$$

In addition, the linear interactions among these five variables are also examined via scatter plots. As an example, Fig. 8(a) and 8(b) show the scatter plots of K_{tr} and c/d versus the actual response y, respectively; and Fig. 8(c) shows the interaction term, K_{tr}·c/d, versus y with a fitted logistic curve. These three plots in Fig. 8 show that although the individual variables might not contribute to the failure mode prediction,

Table 2
Potential variables used for model development.

Term types	x_i				
Single variable	f'_c	c/d	K_{tr}	Q	MC
Interaction of 2 variables	$K_{tr}{\cdot}c/d$	$K_{tr}{\cdot}Q$	$K_{tr}{\cdot}f'_c$	$K_{tr}{\cdot}MC$	$c/d{\cdot}Q$
	$c/d{\cdot}MC$	$c/d{\cdot}f'_c$	$Q{\cdot}MC$	$Q{\cdot}f'_c$	$MC{\cdot}f'_c$
Interaction of 3 variables	$K_{tr}{\cdot}c/d{\cdot}Q$	$K_{tr}{\cdot}Q{\cdot}MC$	$K_{tr}{\cdot}c/d{\cdot}MC$	$K_{tr}{\cdot}c/d{\cdot}f'_c$	$K_{tr}{\cdot}Q{\cdot}f'_c$
	$K_{tr}{\cdot}MC{\cdot}f'_c$	$c/d{\cdot}Q{\cdot}MC$	$c/d{\cdot}Q{\cdot}f'_c$	$c/d{\cdot}MC{\cdot}f'_c$	$Q{\cdot}MC{\cdot}f'_c$
Interaction of 4 variables	$K_{tr}{\cdot}c/d{\cdot}Q{\cdot}MC$	$K_{tr}{\cdot}c/d{\cdot}Q{\cdot}f'_c$	$K_{tr}{\cdot}c/d{\cdot}MC{\cdot}f'_c$	$K_{tr}{\cdot}Q{\cdot}MC{\cdot}f'_c$	$c/d{\cdot}Q{\cdot}MC{\cdot}f'_c$
Interaction of 5 variables	$K_{tr}{\cdot}c/d{\cdot}Q{\cdot}MC{\cdot}f'_c$				

Table 3
Four possible prediction outcomes.

Failure mode	Predicted to be pull-out	Predicted to be splitting
Pull-out ($Y=1$)	True positive (TP)	False negative (FN)
Splitting ($Y=0$)	False positive (FP)	True negative (TN)

their interaction might. Table 2 lists all the potential variables, x_i, used in Eq. (6) for the model development using logistic and lasso classification.

3.3.2. Model prediction accuracy

Different quantities are adopted to measure the performance of the developed models, such as the mean absolute error of prediction, *MAE*:

$$MAE = \frac{\sum_{i=1}^{n}|y_i - \hat{y}_i|}{n} = \frac{\sum_{i=1}^{n}|e_i|}{n} \tag{10}$$

where $\hat{y}_i$ is the prediction, y_i is the true value, and n is the number of data points. Another way to measure prediction accuracy is the hit-or-miss approach. Using the prediction probability formula from Eq. (6) and opting a threshold level of α (that is set to be 50% in this study), then $P(Y=1|\mathbf{x}) \geq \alpha$ indicates a pull-out failure and $P(Y=1|\mathbf{x}) < \alpha$ indicates a splitting failure. Accordingly, based on the correct or wrong prediction of the failure mode, there are four possible outcomes as shown in Table 3: true positive (TP) and true negative (TN) as the correct detections, and false positive (FP) and false negative (FN) as the false detections. Then the probability of correct detection, P_{CD}, as a measure of model prediction accuracy, can be calculated using the number of TP tests (n_{TP}), the number of TN tests (n_{TN}), and the total number of tests (n_{total}):

$$P_{CD} = \frac{n_{TP} + n_{TN}}{n_{total}} \tag{11}$$

Similar measurements can be used for pull-out and splitting failure mode, separately, as follows:

$$P_{CD,pull-out} = \frac{n_{TP}}{n_{TP} + n_{FP}} = \frac{n_{TP}}{n_{pull-out}} \tag{12}$$

and

Table 5
Logistic model coefficients.

Model coefficients	β_0 (Intercept)	β_1 ($c/d{\cdot}Q$)	β_2 ($c/d{\cdot}f'_c$)	β_3 ($Q{\cdot}MC{\cdot}f'_c$)
Mean	−3.46	−4.00	+0.031	0.65
Standard deviation	0.81	1.62	0.008	0.14
Coefficient of variation	−0.23	−0.40	0.25	0.21

$$P_{CD,splitting} = \frac{n_{TN}}{n_{TN} + n_{FN}} = \frac{n_{TN}}{n_{splitting}} \tag{13}$$

3.3.3. Model selection

When using all the 31 variables (listed in Table 2) in Eq. (6), the model is considered as a full model with a model size of 31. For logistic classification, a model selection is performed to the full model to remove the variables with insignificant contributions to the model prediction. In particular, the all possible subset approach [34] is adopted in which all potential combinations of x_i are first formulated for every reduced model size (ranging from 1 to 30), which will result in more than two billion possible models. To keep the model practical, the maximum model size is capped at four (i.e., four variables in a model), which also greatly reduces the computational time. Accordingly, all subsets with model size of five and above are excluded.

In addition, the models with any model parameters having *p*-values greater than 10% and variance inflation factors (*VIFs*) greater than 10 are treated as invalid and are eliminated. Statistical measurements such as *R*-squared (*R-sq*), adjusted *R*-squared (*Adj-R-sq*), and Akaike information criterion (*AIC*) are then used for each model size to evaluate the performance of models.

Models with the highest *R-sq* and *Adj-R-sq* or the lowest *AIC* are the most favorable model for a specific model size. The most favorable models from each subset are then compared to determine the final model. It is noted that different statistical measurements (*Adj-R-sq*, *R-sq*, and *AIC*) may result in a different best model.

The most desirable models for various model sizes are shown in Table 4. *MAE* and P_{CD} are also calculated to compare the performance of those models. It can be observed that the model with a model size of 4 has improved accuracy regarding *R-sq* and *Adj-R-sq*; the model with a model size of 3 has the same accuracy in terms of *MAE* and slightly improved accuracy regarding P_{CD}. Thus, the smaller model size is preferred, and z in Eq. (6) for logistic regression is written as:

$$z = \beta_0 + \beta_1(c/d{\cdot}Q) + \beta_2\left(f'_c{\cdot}c/d\right) + \beta_3\left(Q{\cdot}MC{\cdot}f'_c\right) \tag{14}$$

The statistics of the model coefficients in Eq. (14) are summarized in Table 5.

The method of cross-validation is used to train and validate the lasso model. Cross-validation method divides train set into m folds (10 folds is used in this research), then the model parameters are evaluated through a subsequence manner for various penalty factor values (λ), meaning that in the sparse regularization the independent variables having a corresponding coefficient of zero are eliminated for a given penalty factor value. Hence there will be a subsequence of models having different model sizes associated with the continuance of the penalty factor value. The model with the minimum average deviance plus one standard deviation is suggested to be the final model [32], since this model will balance the prediction that is measured by deviance as

Table 4
Statistics summary for the top three logistic classification models for each model size.

Model size	Independent variables				*R-sq* (%)	*Adj-R-sq* (%)	*AIC*	*MAE*	P_{CD} (%)
1	$c/d{\cdot}MC{\cdot}f'_c$				21	20	13.4	0.48	66
2	$c/d{\cdot}f'_c$	$MC{\cdot}f'_c$			30	27	124.8	0.42	75
3	$c/d{\cdot}Q$	$c/d{\cdot}f'$	$Q{\cdot}MC{\cdot}f'_c$		32	30	123.3	0.33	79
4	MC	$c/d{\cdot}f'_c$	$K_{tr}{\cdot}Q{\cdot}MC$	$Q{\cdot}MC{\cdot}f'_c$	35.2	32	122.5	0.33	78

Table 6
Lasso model coefficients.

Model coefficients	β_0 (Intercept)	β_1 ($MC{\cdot}f'_c$)	β_2 ($c/d{\cdot}f'_c$)	β_3 ($Q{\cdot}MC{\cdot}f'_c$)
Mean	−4.5	0.049	0.014	0.0194
Standard deviation	0.26	0.003	0.001	0.019
Coefficient of variation	−0.06	0.06	0.08	0.97

opposed to false discovery.

Since the method of cross-validation randomly divides data, there is a possibility that each analysis leads to a different result. Thus, the analyses are performed multiple times on the total dataset (100 times in this study). The variables selected at the end of each analysis that appear most frequently among all the repetition is the one selected as the final term. As the result of the multiple analyses conducted in this study, four terms appear most frequently: three terms (i.e., $c/d{\cdot}f'_c$, $MC{\cdot}f'_c$, $Q{\cdot}MC{\cdot}f'_c$) appear in all analyses, and one term (i.e., $K_{tr}{\cdot}c/d{\cdot}f'_c$) appear in half of the analyses. However, when using all these four terms, the accuracy of the resulting model was found to be lower than that for a model using only three terms (i.e., $c/d{\cdot}f'_c$, $MC{\cdot}f'_c$, $Q{\cdot}MC{\cdot}f'_c$); thus, $K_{tr}{\cdot}c/d{\cdot}f'_c$, is excluded. Accordingly, based on lasso classification, z in Eq. (6) can be written as:

$$z = \beta_0 + \beta_1\left(c/d{\cdot}f'_c\right) + \beta_2\left(MC{\cdot}f'_c\right) + \beta_3\left(Q{\cdot}MC{\cdot}f'_c\right) \quad (15)$$

The estimated model coefficients in Eq. (15) are provided in Table 6.

3.4. Model comparison

Using either logistic or lasso classification, both Eq. (14) and Eq. (15) suggest that four independent variables contribute to the failure mode prediction: f'_c, c/d, Q, and MC. It is worthy to understand how these four variables contribute to the bond failure mode. Recall that splitting bond failure involves the radial splitting of the concrete cover by the wedge action of the bar ribs, while pull-out bond failure mainly involves the shearing of the bar against the surrounding concrete. As concrete compressive strength, f'_c, is directly correlated to concrete tensile splitting resistance and shearing cracking resistance, it is not surprising that f'_c is selected in the proposed formulation. Cover to rebar diameter ratio, c/d, was found in many previous literature as an important factor to affect failure mode [35–38], as it measures the confinement around the test bars that could help effectively prevent the splitting cracking in concrete.

The impact of corrosion of rebar, Q, on the bond failure mode, on the other hand, changes the failure mode by changing the interactive effect of ribs and concrete. The produced layer of rust (i.e., steel oxidizes) within the gap between rebar and concrete could act as a lubricant and thus alter the failure mode, mostly from splitting to pull-out [5,6]. Lastly, the loading type of the specimen, monotonic and cyclic, MC, was also found to be a contributing factor in the response of the bond behavior. This is because the cycles in cyclic loading can weaken the bond on each cycle before rupture without causing extensive splitting cracks in concrete [35], which leads to the bond failing in a pull-out

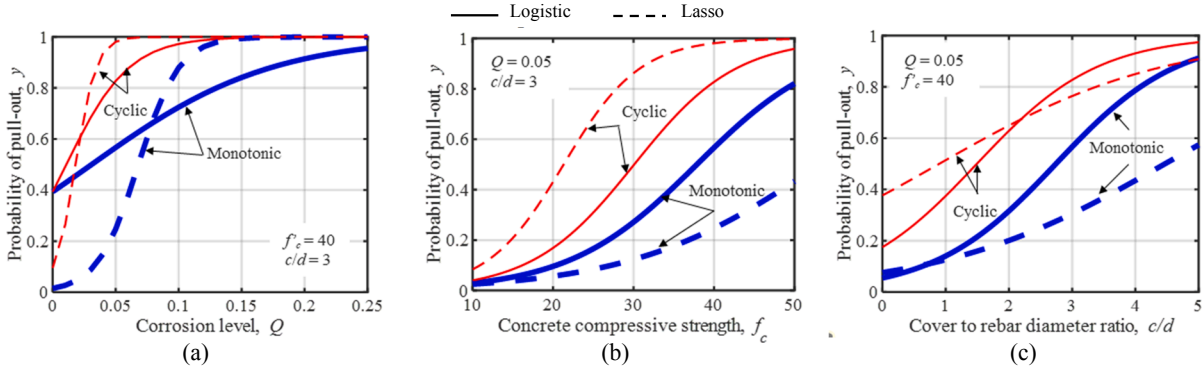

Fig. 9. Sensitivity comparison between logistic and lasso logistic models for (a) corrosion level, (b) concrete compressive strength, and (c) ratio of cover to rebar diameter.

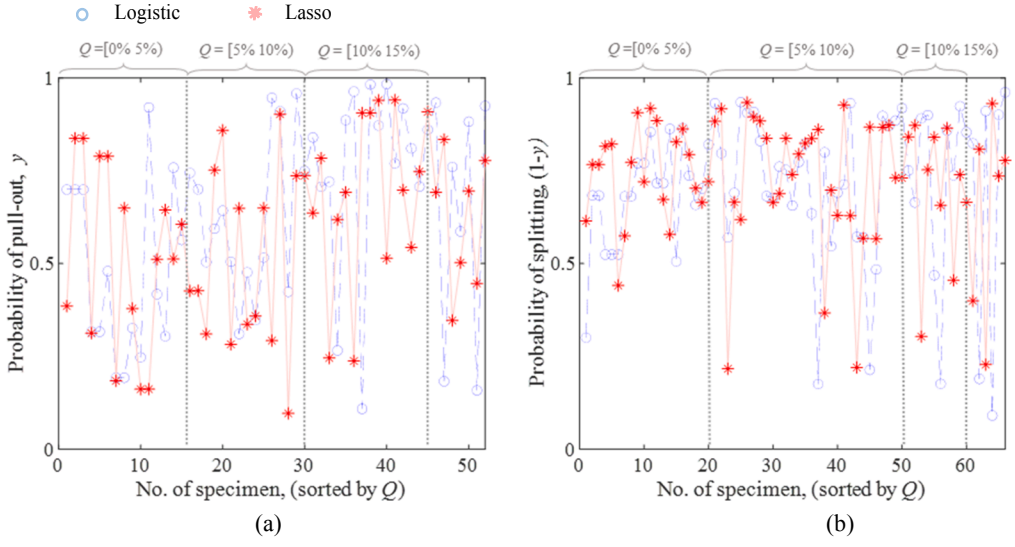

Fig. 10. Prediction plot for (a) pull-out failure and (b) splitting failure.

Table 7
Predictive accuracy of various prediction methods.

	Prediction method	$P_{CD,pull-out}$ (%)	$P_{CD,splitting}$ (%)	P_{CD} (%)	*MAE*
Deterministic methods	CEB [15]	35	59	47	0.72
	ACI-318 [44]	41	58	49	0.75
Classification methods	Logistic	69	84	78	0.34
	Lasso	65	90	80	0.31
	Decision Tree	81	90	85	0.35
	Discriminant	69	88	79	0.36
	k-nearest	56	91	63	0.4
	Naïve Bayes	77	76	76	0.38
	Random forest	94	75	80	0.33
	Support vector machine	86	74	78	0.4

fashion.

In addition, when comparing the selected terms in the logistic and lasso model formulations, it was found that they both include two terms ($c/d{\cdot}f'_c$ and $Q{\cdot}MC{\cdot}f'_c$) and have a negative intercept β_0. Note that both models do not select any terms that include K_{tr}. This finding shows that within the ranges of K_{tr} considered in this study, the transverse stirrup does not influence the failure mode prediction. This is consistent with the findings from Lin et al. [39]. In addition, Soraghi and Huang [7] also found that the presence of a higher amount of transverse stirrups will not necessarily lead to pull-out failure.

Fig. 9 shows the comparison for the sensitivity of the two models to three parameters: Q, f'_c, and c/d under monotonic or cyclic loading. For all three parameters, both models show the same trend: the model prediction for the model under cyclic loading is more sensitive to the x-axis quantity than the one under monotonic loading, which is in agreement with the finding of Kivell et al. [5]. In addition, Fig. 9 indicates that with an increase in Q, f'_c, or c/d, the probability of the failure being pull-out increases; the result regarding corrosion is also consistent with the previous finding from Kivell et al. [5]. However, under cyclic loading, the lasso model is found to be more sensitive than the logistic model with respect to Q (Fig. 9(a)) and f'_c (Fig. 9(b)). Under monotonic loading, the logistic model is found to be more sensitive than the lasso model with respect to f'_c (Fig. 9(b)) and c/d loading (Fig. 9(c)).

Fig. 10 shows a comparison for the predicted probabilities for the specimens based on the developed logistic model (denoted as 'o') and the lasso model (denoted as '*'). For probability prediction, if pull-out failure and splitting failure (shown in Fig. 10(a) and 10(b), respectively), the probability value of the y-axis is closer to one, yielding a better prediction. Overall, for most cases, the predictions from both models are fairly close, and both models provide better predictions for the splitting failure specimens. At lower corrosion levels (less than 10%), the prediction discrepancy between the predictions from the two models seems to be smaller, especially for the splitting failure mode.

Next, the prediction performance of the probabilistic models based on logistic and lasso classification is compared with other methods of classification and the two deterministic models in terms of *MAE*, P_{CD}, $P_{CD,pull-out}$, and $P_{CD,splitting}$. Note that to calculate P_{CD} for the deterministic criteria of CEB (Eq. (4)), Eq. (11) does not consider the cases if the criteria indicate unknown. Thus, to calculate P_{CD}, a 50% of correct detection (i.e. reflecting a random guess) is assigned for the unknown cases. The prediction accuracy comparison is summarized in Table 7. It can be seen that the deterministic models (i.e., CEB and ACI-318) have much lower P_{CD} values and higher *MAE* values compared to the classification methods, indicating a poor prediction capability. On the other hand, the performance of all the classification methods is reasonably close. While the accuracies of the logistic and lasso models are not among the highest in terms of $P_{CD,pull-out}$, they both perform fairly well in terms of $P_{CD,splitting}$, and P_{CD}. In addition, the lasso classification performs best in terms of *MAE*.

As mentioned earlier, classification techniques other than logistic and lasso classification do not result in an explicit formulation. Thus, the logistic and lasso models are still preferred, considering their comparable performance to other classification techniques. In addition, as the lasso model shows better accuracy than the logistic model in terms of *MAE* and P_{CD}, the model based on lasso classification is suggested to be used for the failure mode prediction.

4. Case study

Corrosion of steel reinforcement is one of the main deterioration mechanisms in RC structure performance, as it changes the material properties and weakens the bonding between rebar and concrete. Such deterioration can lead to insufficient rebar development length and, thus, can alter the performance and failure mode of the structure [6,40–42]. Since the investigation has shown that corrosion of rebar may change the bond failure mode as shown in the developed probabilistic models, it is worth attempting to evaluate the impact of corrosion on the structural performance.

In the literature, four-point testing is typically adopted by researchers to study rebar-concrete bond behavior. In this study, an RC beam with a lap splice studied by Abdel-Kareem et al. [43] is adopted to investigate how corrosion might impact the reliability of the beam flexural performance under a four-point lording through its impact on the bond failure mode. The geometry and reinforcement detailing of this beam are shown in Fig. 11. The support-to-support length of the beam is 3000 mm. Transverse stirrups with 100 mm spacing and a diameter of 8 mm are provided along the beam to avoid shear failure. As shown in Fig. 11, the lap-spliced rebar is distributed along with the constant moment region. The lap splice l_s is calculated using ACI 318 [44], resulting in $l_s = 542$ mm. The related equations for calculating l_s are provided in Appendix C. In addition, the concrete compressive strength,

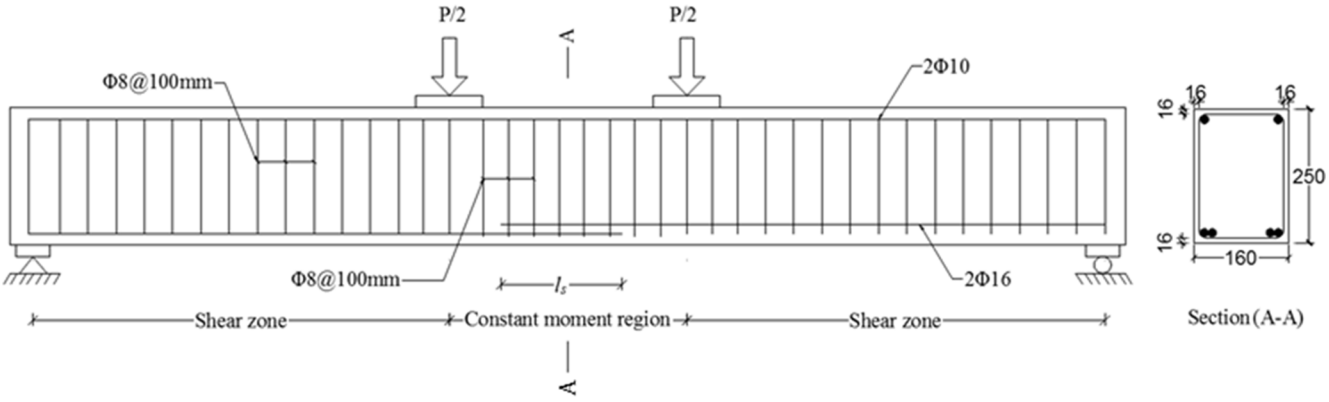

Fig. 11. Cross-section and longitudinal detailing of the beam (dimensions are in mm) [43].

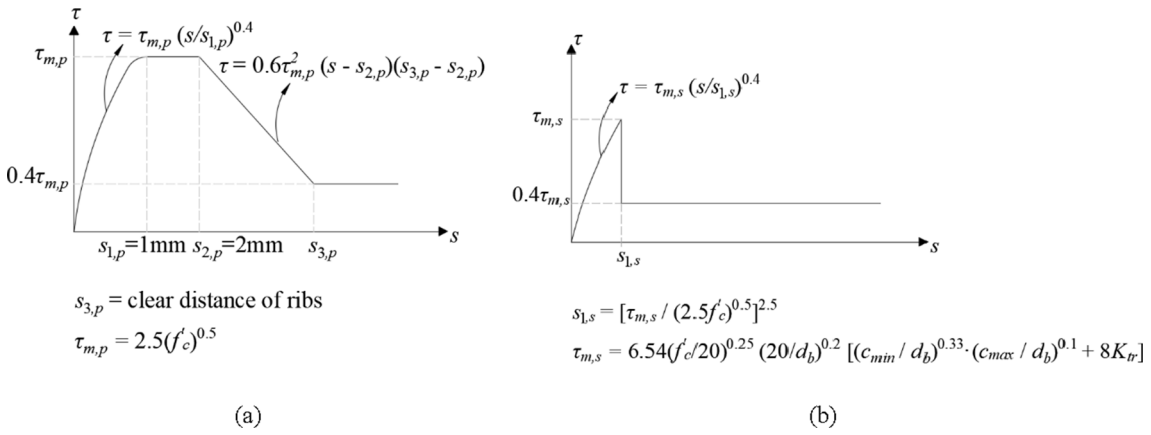

Fig. 12. Adopted bond-slip curve based on CEB for (a) pull-out failure mode and (b) splitting failure mode [15].

f'_c, is assumed to be 40 MPa.

In order to incorporate the stress-slip bond behavior, the nonlinear load-deflection behavior of the RC beams is obtained through an analytical procedure proposed by Sajedi and Huang [45]. This analytical procedure can be applied to lap-spliced beams or beams without lap splice, taking into account the effects of corrosion on the diameter of the reinforcements, the yield strength of bars, and the stress-slip bond behavior at the rebar-concrete interface. This procedure utilizes the extension of steel reinforcement between flexural cracks that considers the bond-slip behavior at the rebar-concrete interface to estimate the nonlinear force-displacement of RC beams. The detailed information about this procedure is summarized in Appendix D. Next, the analytical procedure is embedded in the first-order reliability analysis (FORM) to obtain the probability of failure.

The bond behavior under pull-out or splitting failure used in the analytical procedure is based upon the stress-slip curve in the CEB code [15], where bond stress, τ, between rebar and concrete is determined as a function of relative slippage, s, as illustrated in Fig. 12, where τ_m is the maximum bond stress (i.e., bond strength) and s_1 is the slippage when $\tau = \tau_m$. It is worth to note that the prediction performance of the CEB criteria for bond failure mode is not very good at all as shown in Table 9, but the CEB bond stress-slip model formula has been widely accepted and validated by many previous literature [46–52], and this stress-slip formula shown in Fig. 12 is consequently adopted in this research.

To consider the effect of corrosion, the bond strength is calculated using a model previously developed by Sajedi and Huang [13], as shown in Eq. (D.2) in Appendix D. Since Eq. (D.2) is developed based on the specimens that failed in splitting failure modes, it can be used for assessing bond strength under splitting failure, $\tau_{m,s}$, not for bond strength under pull-out failure, $\tau_{m,p}$. By utilizing the ratio of the bond strength for pull-out failure (i.e., $8.0(f'_c/20)^{0.25}$) to the bond strength for splitting failure (i.e., $2.5f'^{0.5}_c$) as suggested by CEB [15], $\eta = 8.0(f'_c/20)^{0.25}/(2.5f'^{0.5}_c)$, one can set $\tau_{m,p} = \eta \cdot \tau_{m,s}$.

4.1. Flexural behavior

Four levels of corrosion are studied and compared: 0% (intact beam), 5%, 10%, and 15%. First, the flexural behaviors for the intact and corroded RC beams under four-point loading are compared through deterministic analyses that consider the bond pull-out behavior and splitting behavior separately. Three criteria are used to stop the analysis as a flexural failure: the first criterion is when the ultimate bond stress, τ_u, becomes larger than the bond strength, τ_m ($\tau_u > \tau_m$); the second criterion is when the concrete reaches its allowable strain (i.e., $\varepsilon_{concrete} > 0.0038$), at which point the concrete is considered to fail by crushing; and the third criterion is when the rebar stress reaches its ultimate tensile strength ($f_s > f_u$). Notice that the third failure criterion never occurred in the case study. Also, note that these failure scenarios (e.g., bond failure and concrete crushing) could occur before or after rebar yielding, and rebar yielding itself does not indicate a beam failure in this study.

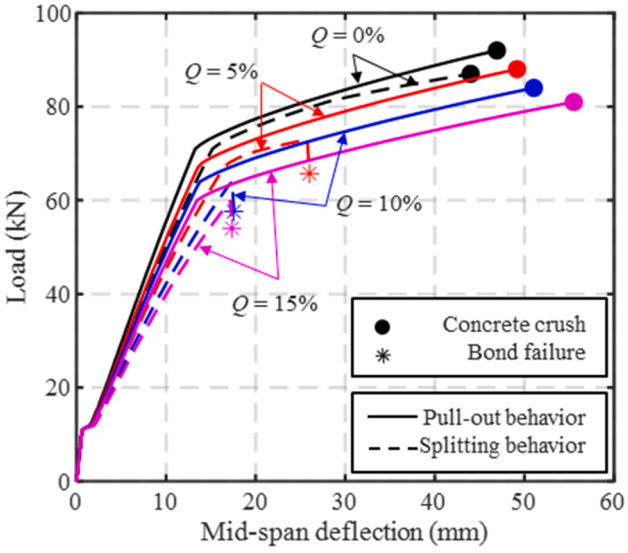

Fig. 13. Comparison of pull-out and splitting failure for different levels of corrosion.

Table 8
Beam flexural behavior comparison for different scenarios.

Corrosion level, Q	Bond behavior	E	F_y	Δ_y	F_u	Δ_u	$\mu = \Delta_u/\Delta_y$	F_u/F_y
Intact beam	Pull-out	5.3	71	13.2	92	46.9	3.5	1.3
	Splitting	4.4	71	15.1	92	60.8	4.0	1.3
Q = 5%	Pull-out	4.9	67	13.5	88	49.1	3.6	1.3
	Splitting	3.8	67	17.6	73	25.7	1.5	1.1
Q = 10%	Pull-out	4.6	64	13.7	84	51.1	3.7	1.3
	Splitting	3.6	–	17.4	64	–	<1	–
Q = 15%	Pull-out	5	60	13.4	81	55.5	4.1	1.35
	Splitting	3.78	–	17.7	60	–	<1	–

Fig. 13 shows the force-displacement curves for the RC beams and Table 8 summarizes the characteristics of the flexural behavior: modulus before yielding (E), yielding force (F_y), yielding displacement (Δ_y), rupture force (F_u), ultimate displacement (Δ_u), ductility (Δ_u/Δ_y), and hardening ratio (F_u/F_y). The results from both Fig. 13 and Table 8 show

that the structure performs differently when bond behaviors are in pull-out mode or splitting mode. Such a difference becomes more apparent when the corrosion level is increased.

For the beams with the same level of Q except for $Q = 15\%$, F_y is about the same regardless of the bond behavior. A beam with pull-out bond behavior will have a higher modulus, a higher ductility, and a higher hardening ratio as shown in Table 8. As expected, the performance of the beam with pull-out bond behavior is more desirable. In the flexural curves shown in Fig. 13, the stiffness of the beam initially changes when the load reaches around 11 kN, and this change at the beginning of the curve is due to the creation of initial cracks in the concrete considered in the analytical formulation. Furthermore, when the beam is under pull-out bond behavior, the flexural failure ends with concrete crushing; however, when the beam is under splitting bond behavior, the beam fails in bond except for the intact case. More importantly, for the beams with corrosion levels of 10% and 15% under splitting bond behavior, the bond failure occurs prior to yielding, which is a brittle failure, not a desirable type of failure.

To avoid such brittle failure, one could increase the splice length as the value suggested by ACI 318 does not appear to be sufficient when corrosion is present [53] or design the beam so that the bond will exhibit in a pull-out behavior. To ensure pull-out bond behavior, one could utilize the proposed model shown in Eq. (15) that is determined by four variables f'_c, c/d, Q, and MC. In particular, one could determine the values of the two design parameters, f'_c, and c/d, in order to ensure the desired probability level of achieving pull-out bond, with the consideration of the corrosion and loading scenarios that could happen in the service life.

4.2. Reliability analysis

To evaluate the reliability of the beam flexural performance, the probability of failure is calculated as:

$$P_f = P\left(\bigcup_k g_k \leqslant 0\right) \tag{16}$$

where g_k is the limit-state function corresponding to the failure mode k and the subscript k denotes the failure mode of the beam (1 for bond being pull-out and 2 for bond being splitting). The limit state function is defined by:

$$g_k = C_k(\boldsymbol{x}_r) - D \tag{17}$$

where $C_k(\cdot)$ refers to the capacity of the beam; $\mathbf{x}_r$ is a random variable vector that includes all basic random variables such as material properties and geometric dimensions, and D is the force demand applied to the structure. Since bond behavior being pull-out or splitting are two mutually exclusive events, Eq. (16) can be written as:

$$\begin{aligned} P_f = {} & P[(C_1(\boldsymbol{x}_r) - D \leqslant 0 | Y = 1)] \cdot P(Y = 1) \\ & + P[C_2(\boldsymbol{x}_r) - D \leqslant 0 | Y = 0] \cdot P(Y = 0) \end{aligned} \tag{18}$$

where $P(Y = 1)$ and $P(Y = 0) = 1 - P(Y = 1)$ refer to the probability of the bond being a pull-out behavior or a splitting behavior, respectively, which can be calculated based on the developed model shown in Eq. (6) and Eq. (14). The capacity $C(\mathbf{x}_r)$, which is the maximum force the beam can resist before flexural failure is obtained from the analytical procedure in Appendix D. Note that when the failure occurs, it does not necessarily indicate bond failure. In practice, the reliability index, β, is typically used as the performance measure, and its relationship with P_f is as follows:

$$P_f = \Phi(-\beta) \tag{19}$$

The basic random variables, $\mathbf{x}_r$, are adopted based on the literature [53,54] and their probability information is provided in Table 9. Note that the model error, $\sigma\varepsilon$, in Table 9 refers to the model error in the bond strength model adopted from the literature [13] that is elaborated in Appendix D.

Table 9
Probability information of the basic random variables.

Type	Random variable	Distribution (Mean*, std.)	Importance measure ($Q = 5\%$, $D = 60$ kN)	
			Pull-out	Splitting
Geometrical	d_b (mm)	Normal (16, 0.32) [54]	0.078	0.031
	h (mm)	Normal (250, 2.5) [54]	−0.061	0.078
	b (mm)	Normal (160, 0.32) [54]	0	0
	C_x (mm)	Normal (16, 1.92) [53]	0	0
	C_t (mm)	Normal (16, 1.92) [53]	0	0
	C_b (mm)	Normal (16, 1.92) [53]	0	0
	d_{st} (mm)	Normal (8, 0.16) [54]	0	0
Mechanical	f_y (MPa)	Normal (440, 22) [53]	0.121	0.156
	f_c (MPa)	Normal (40, 7.2) [53]	−0.729	−0.470
	$f_{y,st}$ (MPa)	Normal (280, 14) [53]	0	0
Model error	$\sigma\varepsilon$	Normal (0, 0.169) [53]	−0.668	−0.861

The contribution of each random variable to the variability of the limit state function (Eq. (17)) is also investigated based on the important measures of the random variables when considering 5% corrosion and a demand of 60 kN, and the results are shown in Table 9. A larger absolute value of importance measure indicates a greater contribution of the corresponding random variable on the variability of the limit state function. The detailed information of importance measures in reliability analysis can be found in related literature [55]. Table 9 shows that for both cases (bond behaves in splitting and in pull-out), three variables, model error in bond strength, f_y, and f'_c (namely bond, concrete, and steel properties) dominates the contribution to the variability of the limit state function.

Fig. 14 shows the fragility curves conditioned on demand values with corrosion levels of 0% (intact beam), 5%, 10%, and 15%. For a given level of corrosion, the fragility curves show the differences in the structural performance due to different bond

behaves in pull-out, splitting, or unknown (that is determined by the developed bond failure prediction model), and these differences become more apparent with the increase in corrosion.

For the bond failure modes at each considered probability, the fragility curve for unknown bond failure mode (shown as a dotted line) is between the fragility curves for the bond in pull-out behavior (shown as a solid line) and the bond in splitting behavior (shown as a dashed line), as expected. In particular, the fragility curve with the unknown bond is closer to the curve for splitting bond behavior when the corrosion level Q is low, but it moves closer to the curve with pull-out bond behavior when Q increases. This is understandable, as the probability of being pull-out increases with the level of corrosion (as shown in Fig. 14).

While compares the four plots in Fig. 14, the fragility curves with a given bond behavior shift to the left as Q increases. This shows the corrosion increases the probability of failure as expected. In particular, the fragility curves for splitting bond behavior are more distant from each other with the increase of Q. For example, at the lowest level of corrosion ($Q = 5\%$) shown in Fig. 14(b), the fragility curve for splitting failure is significantly distant from the curve for the intact beam shown in Fig. 14(a). However, the fragility curves for pull-out bond behavior do not change dramatically with the change of Q. This indicates that corrosion has more impact on the performance of a structure with a splitting bond than the structure with a pull-out bond. It can also be seen that with the increase of the corrosion level, the fragility curves became steeper, indicating that the probability of failure becomes more sensitive to demand with more corrosion.

Fig. 15 (a) and (b) show the reliability index curves with respect to the level of corrosion Q by setting the demand D as a deterministic value of 60 kN and as a random variable with mean $\mu_D = 60$ kN and COV =

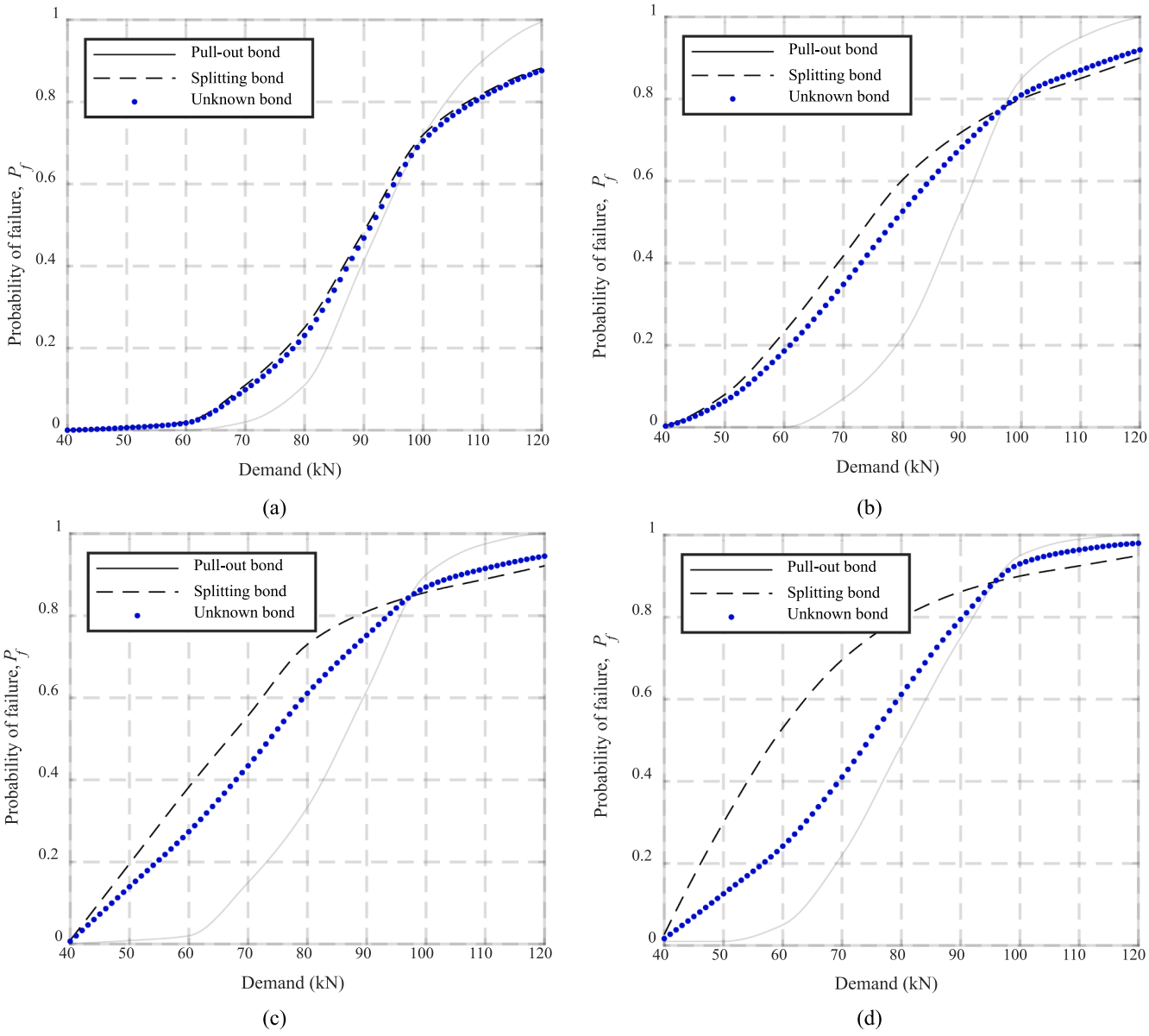

Fig. 14. Fragility curves under different corrosion levels: (a) $Q = 0\%$ (intact beam), (b) $Q = 5\%$, (c) $Q = 10\%$, and (d) $Q = 15\%$.

0.15, respectively. The purpose of Fig. 15 is to examine how the bond behavior impacts the structural performance with a progressing deterioration; thus, the demand used in Fig. 15 can be arbitrary. Moreover, the reliability index curve with the unknown bond failure mode is between the other two curves. The reliability index curve with splitting bond behavior is much lower than the one with pull-out bond behavior, and its rate of decrease is much greater. From $Q = 0\%$ to $Q = 5\%$, β decreases from 3.3 to 1.8 in Fig. 15(a) and decreases from 3.1 to 2.1 in Fig. 15(b). Consistent with the previous observations in Figs. 13 and 14, the result from both Fig. 15(a) and (b) indicates that the bond behavior plays a critical role in the time-dependent performance evolution, particularly when the specimen is exposed to a high level of corrosion. In addition, the prediction of the bond failure behavior is important, as it determines the actual structural performance.

5. Summary and conclusions

Sufficient bonding of rebar to concrete is crucial to ensure the reliable performance of RC structures, particularly in the corroded structures. Whilst much research has investigated the bond strength, estimation of the bond failure mode (i.e. pull-out or splitting) considering corrosion has been given little attention. In this study, by taking advantage of machine learning classifications, a probabilistic model was developed to estimate the bond failure mode. specifically, logistic and lasso classification techniques are found to be suitable for engineering practice, as they provide explicit formulations. The developed model is based on the results of bond tests for 132 beam-end specimens with various influencing parameters such as concrete compressive strength, rebar diameter size, cover size, corrosion level, and loading type (i.e., monotonic or cyclic). To evaluate if the bond behavior under corrosion affects the performance of a structure, the flexural performance of an RC beam with a lap splice under various levels of corrosion is evaluated by conducting a reliability analysis. The main findings of this study are summarized as follows:

- Machine learning approaches such as logistic and lasso classification techniques provide probabilistic predictions of categorical variables such as the bond failure mode, and they provide explicit and easy-to-implement formulations for engineering practice.

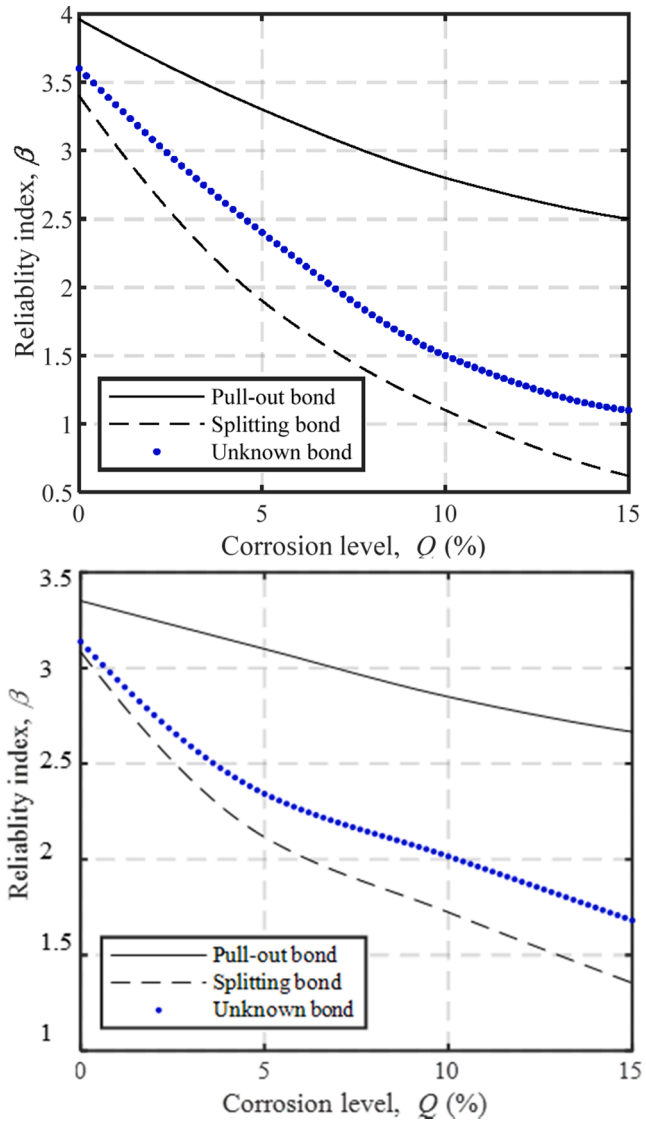

Fig. 15. Reliability index curves under various corrosion levels conditioned on different bond behaviors under (a) $D = 60$ kN and (b) $\mu_D = 60$ kN and COV = 0.15.

- Both logistic and lasso classification methods have similar prediction performances: much better than the deterministic approaches and not worse than most of the other classification methods; however, lasso classification is found to be more accurate.
- The parameters that influence the bond failure mode prediction are concrete compressive strength, cover to the rebar diameter ratio, corrosion level, and loading type (cyclic or monotonic).
- Based on the developed probabilistic prediction models, the amount of transverse stirrup does not influence the bond failure mode.
- At the structural level, the flexural performance of the beam in the case study shows the dependence on the bond behavior, and more so at higher levels of corrosion. In addition, for high levels of corrosion where the beams exhibit splitting bond behavior, the beam fails brittlely (that is failure occurs prior to rebar yielding), which is not a desirable type of structural failure.
- The case study also shows that bond behavior has a great impact on the structural reliability index curves, and more so as the level of corrosion increases. Thus, the prediction of the bond failure mode is critical for time-dependent reliability-based analysis.

Data availability statement

The raw/processed data required to reproduce these findings cannot be shared at this time as the data also forms part of an ongoing study.

Funding

This material is based upon work supported by the National Science Foundation under Grant No. CMMI 1635507. Any opinions, findings, and conclusions or recommendations expressed in this material are those of the authors and do not necessarily reflect the views of the National Science Foundation.

CRediT authorship contribution statement

Ahmad Soraghi: Conceptualization, Formal analysis, Investigation, Methodology, Software, Validation, Visualization, Writing - original draft, Writing - review & editing. **Qindan Huang:** Conceptualization, Funding acquisition, Investigation, Methodology, Project administration, Resources, Supervision, Validation, Visualization, Writing - original draft, Writing - review & editing.

Table A1
Specimen specifications (group 1).

Group	No.	Rebar diameter, d_b [mm]	Loading type*	f'_c [MPa]	Bond length, l_b [mm]	Cover, c [mm]	c/d	K_{tr}	Q_{target} (%)	Q_{actual} (%)	Failure Mode**
Group 1	1	15.875	M	43	88.9	50.8	3.20	0.00	0%	0.0%	S
	2					63.5	4.00	0.00	10%	4.9%	P
	3					76.2	4.80	0.00	20%	7.6%	S
	4					50.8	3.20	5.89	0%	0.0%	P
	5					63.5	4.00	5.89	10%	5.3%	P
	6					76.2	4.80	5.89	20%	9.9%	P
	7		C			50.8	3.20	0.00	0%	0.0%	S
	8					25.4	1.60	0.00	5%	10.3%	P
	9					63.5	4.00	0.00	10%	11.0%	P
	10					38.1	2.40	0.00	15%	10.1%	P
	11					76.2	4.80	0.00	20%	12.0%	P
	12					50.8	3.20	5.89	0%	0.0%	P
	13					25.4	1.60	5.89	5%	7.9%	NA
	14					63.5	4.00	5.89	10%	4.3%	P
	15					38.1	2.40	5.89	15%	8.2%	S
	16					76.2	4.80	5.89	20%	11.3%	P
	17	19.05	M		114.3	38.1	2.00	0.00	0%	0.0%	S
	18					25.4	1.33	0.00	10%	3.6%	S
	19					50.8	2.67	0.00	20%	15.6%	P
	20					38.1	2.00	4.91	0%	0.0%	P
	21					25.4	1.33	4.91	10%	3.2%	S
	22					50.8	2.67	4.91	20%	7.1%	S
	23		C			38.1	2.00	0.00	0%	0.0%	S
	24					63.5	3.33	0.00	5%	8.5%	NA
	25					25.4	1.33	0.00	10%	7.6%	P
	26					76.2	4.00	0.00	15%	9.9%	S
	27					50.8	2.67	0.00	20%	13.4%	P
	28					38.1	2.00	4.91	0%	0.0%	P
	29					63.5	3.33	4.91	5%	8.6%	P
	30					25.4	1.33	4.91	10%	6.9%	S
	31					76.2	4.00	4.91	15%	7.7%	P
	32					50.8	2.67	4.91	20%	11.0%	P
	33	25.4	M		203.2	63.5	2.50	0.00	0%	0.0%	S
	34					50.8	2.00	0.00	10%	4.3%	S
	35					38.1	1.50	0.00	20%	10.2%	S
	36					63.5	2.50	3.68	0%	0.0%	S
	37					50.8	2.00	3.68	10%	7.7%	S
	38					38.1	1.50	3.68	20%	11.9%	P
	39		C			63.5	2.50	3.68	0%	0.0%	S
	40					50.8	2.00	0.00	10%	5.2%	NA
	41					38.1	1.50	0.00	20%	13.1%	NA
	42					63.5	2.50	3.68	0%	0.0%	NA
	43					50.8	2.00	3.68	10%	5.7%	P
	44					38.1	1.50	3.68	20%	13.7%	P

* M (monotonic), and C (cyclic).
** P (pull-out), S (splitting), and NA (not assigned).

Table A2
Specimen specifications (group 2).

Group	No.	Rebar diameter, d_b [mm]	Loading type*	f'_c [MPa]	Bond length, l_b [mm]	Cover, c [mm]	c/d	K_{tr}	Q_{target} (%)	Q_{actual} (%)	Failure Mode**
Group 2	1	15.875	M	36	88.9	25.4	1.60	11.73	5%	13.1%	P
	2					38.1	2.40	11.73	0%	0.0%	P
	3					38.1	2.40	11.73	10%	16.3%	S
	4					50.8	3.20	11.73	10%	14.9%	P
	5					50.8	3.20	11.73	15%	18.4%	S
	6					63.5	4.00	11.73	5%	13.0%	S
	7					63.5	4.00	11.73	15%	15.9%	S
	8					76.2	4.80	11.73	15%	18.8%	P
	9		C			25.4	1.60	11.73	5%	16.3%	P
	10					38.1	2.40	11.73	0%	0.0%	S
	11					38.1	2.40	11.73	10%	15.7%	S
	12					50.8	3.20	11.73	10%	15.4%	S
	13					50.8	3.20	11.73	15%	17.2%	P
	14					63.5	4.00	11.73	5%	19.1%	P
	15					63.5	4.00	11.73	15%	16.5%	S
	16					76.2	4.80	11.73	15%	15.6%	S
	17	19.05	M		114.3	25.4	1.33	9.78	5%	6.3%	P
	18					38.1	2.00	9.78	0%	0.0%	P
	19					38.1	2.00	9.78	10%	11.2%	P
	20					50.8	2.67	9.78	10%	12.6%	P
	21					50.8	2.67	9.78	15%	25.8%	S
	22					63.5	3.33	9.78	5%	7.1%	P
	23					63.5	3.33	9.78	15%	10.5%	S
	24					76.2	4.00	9.78	15%	10.8%	P
	25		C			25.4	1.33	9.78	5%	6.5%	S
	26					38.1	2.00	9.78	0%	0.0%	S
	27					38.1	2.00	9.78	10%	13.3%	S
	28					50.8	2.67	9.78	10%	12.8%	S
	29					50.8	2.67	9.78	15%	10.3%	S
	30					63.5	3.33	9.78	5%	5.4%	S
	31					63.5	3.33	9.78	15%	12.1%	S
	32					76.2	4.00	9.78	15%	11.4%	S
	33	25.4	M		152.4	76.2	3.00	7.33	5%	6.0%	P
	34					76.2	3.00	7.33	0%	0.0%	P
	35					88.9	3.50	7.33	5%	10.7%	P
	36					88.9	3.50	7.33	10%	7.4%	S
	37					101.6	4.00	7.33	5%	4.9%	P
	38					101.6	4.00	7.33	10%	7.7%	S
	39		C			76.2	3.00	7.33	5%	5.7%	S
	40					76.2	3.00	7.33	0%	0.0%	NA
	41					88.9	3.50	7.33	5%	5.1%	S
	42					88.9	3.50	7.33	10%	7.5%	NA
	43					101.6	4.00	7.33	5%	5.4%	NA
	44					101.6	4.00	7.33	10%	8.1%	S

Table A3
Specimen specifications (group 3).

Group	No.	Rebar diameter, d_b [mm]	Loading type*	f'_c [MPa]	Bond length, l_b [mm]	Cover, c [mm]	c/d	K_{tr}	Q_{target} (%)	Q_{actual} (%)	Failure Mode**
Group 3	1	15.875	M	27	88.9	25.4	1.60	11.73	5%	7.9%	P
	2					38.1	2.40	11.73	0%	0.0%	P
	3					38.1	2.40	11.73	10%	10.3%	S
	4					50.8	3.20	11.73	10%	11.2%	S
	5					50.8	3.20	11.73	15%	6.5%	P
	6					63.5	4.00	11.73	5%	4.8%	S
	7					63.5	4.00	11.73	15%	4.0%	P
	8					76.2	4.80	11.73	15%	7.8%	S
	9		C			25.4	1.60	11.73	5%	6.2%	P
	10					38.1	2.40	11.73	0%	0.0%	P
	11					38.1	2.40	11.73	10%	7.7%	P
	12					50.8	3.20	11.73	10%	9.8%	NA
	13					50.8	3.20	11.73	15%	9.1%	P
	14					63.5	4.00	11.73	5%	3.4%	P
	15					63.5	4.00	11.73	15%	11.9%	NA
	16					76.2	4.80	11.73	15%	16.9%	P
	17	19.05	M		114.3	25.4	1.33	9.78	5%	5.2%	P
	18					38.1	2.00	9.78	0%	0.0%	P
	19					38.1	2.00	9.78	10%	6.2%	S
	20					50.8	2.67	9.78	10%	7.1%	NA
	21					50.8	2.67	9.78	15%	9.0%	P
	22					63.5	3.33	9.78	5%	5.4%	P
	23					63.5	3.33	9.78	15%	9.5%	P
	24					76.2	4.00	9.78	15%	7.2%	P
	25					25.4	1.33	9.78	5%	6.1%	S
	26		C			38.1	2.00	9.78	0%	0.0%	NA
	27					38.1	2.00	9.78	10%	6.8%	P
	28					50.8	2.67	9.78	10%	6.6%	S
	29					50.8	2.67	9.78	15%	5.8%	P
	30					63.5	3.33	9.78	5%	8.0%	S
	31					63.5	3.33	9.78	15%	8.2%	S
	32					76.2	4.00	9.78	15%	8.3%	S
	33	25.4	M		152.4	76.2	3.00	7.33	5%	5.0%	S
	34					76.2	3.00	7.33	0%	0.0%	P
	35					88.9	3.50	7.33	5%	3.7%	S
	36					88.9	3.50	7.33	10%	7.4%	S
	37					101.6	4.00	7.33	5%	4.7%	P
	38					101.6	4.00	7.33	10%	6.7%	S
	39		C			76.2	3.00	7.33	5%	4.7%	P
	40					76.2	3.00	7.33	0%	0.0%	P
	41					88.9	3.50	7.33	5%	4.6%	P
	42					88.9	3.50	7.33	10%	5.9%	P
	43					101.6	4.00	7.33	5%	5.6%	P
	44					101.6	4.00	7.33	10%	5.8%	P

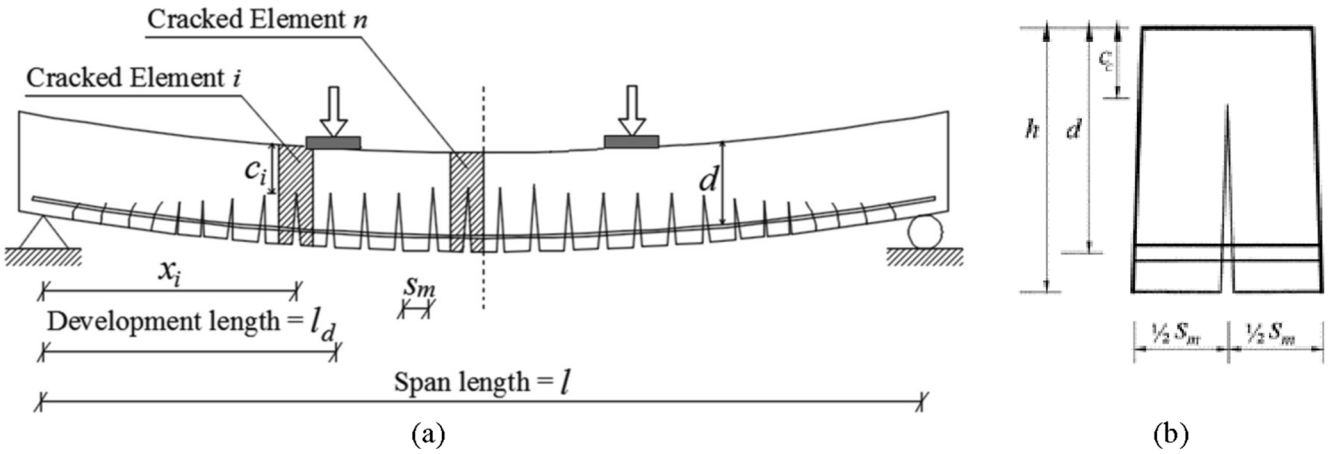

Fig. D1. (a) Typical cracked beam under flexural loading [19], and (b) typical crack element [61].

Declaration of Competing Interest

The authors declare that they have no known competing financial interests or personal relationships that could have appeared to influence the work reported in this paper.

Acknowledgements

This material is based upon work supported by the National Science Foundation under Grant No. CMMI 1635507. Any opinions, findings, and conclusions or recommendations expressed in this material are those of the authors and do not necessarily reflect the views of the National Science Foundation.

Appendix A. Designed specimen specifications

See Tables A1-A3.

Appendix B. Classification algorithms

Decision tree

A decision tree is a decision support, non-parametric method that uses a tree-like model constructed from the training data and includes a sequence of yes/no questions to classify all observations. Hence, the response is predicted using the tree graph. The decision tree consists of nodes and branches in which the nodes belong to the test condition and the branches represent the outcome of the test. By following the nodes and branches of the tree, a decision can be made [56].

Discriminant analysis

In discriminant classification, different classes are assumed to generate data following various Gaussian distributions [57]. Linear discriminant analysis (LDA) and quadratic discriminant analysis (QDA) are two types of discriminant analysis. In LDA Bayes theorem is used to predict the probabilities of the output category, k, into the kth category given the input vector of $\mathbf{x}$ that can be written as:

$$Pr(Y = k|\mathbf{x}) = \frac{\pi_k f_k(\mathbf{x})}{\sum_{l=1} \pi_l f_l(\mathbf{x})} \tag{B1}$$

where π_k is the prior probability (in this study $\pi_k = 0.5$) and $f_k(\mathbf{x})$ refers to the density function of $\mathbf{x}$. In this study, $f_k(\mathbf{x})$ is considered to have a joint normal or Gaussian distribution, and π_k is the prior probability of an observation belonging to the kth class. QDA is similar to LDA in that it assigns inputs to the kth category, but QDA considers each category as having a unique covariance matrix. Accordingly, classes in LDA have a linear boundary and quadratic boundary in QDA. This study adopts QDA for the class boundary due to its better prediction accuracy [58].

K-nearest neighbors classification

K-nearest neighbors (KNN) classification is a non-parametric classification method [59]. Having a test observation of y_0 and K as a positive integer, the KNN determines K observations in the training data nearest to y_0 that are denoted as N_0. It then predicts the conditional probability for class k as the fraction of data points in N_0 as follows:

$$Pr(Y = k|\mathbf{x}) = \frac{1}{K} \sum_{i \in N_0} I(y_i = k) \tag{B2}$$

where $I(\cdot)$ refers to the indicator variable. The main drawback of using the KNN method is that the chosen value of K is sensitive to the prediction

performance. To deal with this issue, the approach of cross-validation is adopted in this study for different values of K, and the best model is selected.

Naïve Bayes classification

Naïve Bayes classification uses the Bayes theorem for classifying data by assigning an observation to a class when the probability belongs to that observation is larger than 50%. By assuming that the input vector $\mathbf{x}$ is independent for a given class, k, the probability of an observation pertains to that class can be formulated as [59]:

$$\Pr(Y=k|\mathbf{x}) = \frac{\Pr(Y=k)\Pr(\mathbf{x}|Y=k)}{\Pr(\mathbf{x})} = \frac{\Pr(Y=k)\prod_{i=1}^{N}\Pr(\mathbf{x}|Y=k)}{\Pr(\mathbf{x})} \tag{B3}$$

Random forest

A random forest includes a group of decision trees in a way that each tree predictor produces a response based on a set of input variables [60]. A random forest creates many learning models (i.e., decision trees) that increase the classification accuracy. This process, also known as *bagging*, works by averaging noisy and unbiased models to create a model with low variance. The prediction of each observation is obtained from average of all decision trees and can be formulated using the following equation:

$$Pr(Y=k|\mathbf{x}) = \frac{1}{B}\sum_{b=1}^{B} f_b(\mathbf{x}) \tag{B4}$$

where B is the number of decision trees and f_b is the decision tree prediction.

Support vector machine

A support vector machine (SVM) is a simple classifier generalization known as a maximal margin classifier for categorization [59]. This model builds a hyper-plane (e.g. a linear or polynomial equation of $\mathbf{x}$) that has the maximum distance from the nearest point of each category based on the training data. SVM is a non-probabilistic classification that constructs a classifier as follows:

$$Pr(Y=k|\mathbf{x}) = sign\left[\sum_{i=1}^{N}\alpha_i y_i \Psi(\mathbf{x},\mathbf{x}_i) + b\right] \tag{B5}$$

in which N is the number of training data, α_i is a positive real factor, and b is a real constant. The parameter $\Psi(\cdot)$ is a defined function: for a linear SVM, $\Psi(\mathbf{x},\mathbf{x}_i) = \mathbf{x}_i^T\mathbf{x}$ and for a polynomial SVM, $\Psi(\mathbf{x},\mathbf{x}_i) = (\mathbf{x}_i^T\mathbf{x}+1)^d$, in which d is an a priori value specified by the user. This study adopted a polynomial SVM to achieve the best accuracy.

Appendix C. Lap splice length

The designed lap splice length for the adopted beam from Abdel-Kareem [43] is from ACI 318-11 design code provisions [44], in which l_d can be calculated as:

$$l_d = \frac{0.9 f_y min(\psi_t,\psi_e,1.7)\psi_s\lambda}{\sqrt{f'_c}\,min(\frac{c+k_{tr}}{d},2.5)}d_b \tag{C1}$$

where Ψ_t, Ψ_e, and Ψ_s are modification coefficients to consider the location of reinforcement effects, coating, and size of reinforcement, respectively; λ is an aggregate concrete factor, and c is the smaller of the distance from the half of center-to-center spacing of the developed bars and the distance from the nearest concrete surface to the center of the rebar (units are based on SI units). K_{tr} is the calculated based on:

$$K_{tr} = \frac{A_{tr}\cdot f_{yt}}{10.34 s\cdot n} \tag{C2}$$

where n is the number of rebars developed within the splitting plane. For the calculation of l_d in Eq. (C.1), the values for the modification factors are $\Psi_t = \Psi_e = \Psi_s = \lambda = 1.0$. Note that to obtain the minimum splice length, l_d can be replaced with l_s [45].

Appendix D. Analytical procedure

As mentioned in Eq. (18), it is necessary to calculate the capacity of the structure. The following procedure is used to obtain the capacity, $C(\mathbf{x}_r)$. In this process, the beam is modeled as a series of elements having the length of crack sizes. The RC beam is assumed to be purely under a constant bending moment. The beam is assumed to have a single crack at its midpoint and, as the bending moments increase, the crack expands toward the supports. The rebar-concrete bonding transfers some portion of the tensile forces created by the bending moment and, thus, reduces the steel elongation and strain within each element, allowing the deflection and rotation be lowered. The midspan deflection, Δ, can be calculated as [61]:

$$\Delta = \sum_{i=1}^{i=n}\frac{e_i}{d-c_c}x_i \tag{D1}$$

where n is the number of cracks, e_i is the elongation of each individual crack, d is the height of the center of the tensile rebar to the top of the concrete section, and c is the difference between the height of the top of the section and the top of the crack in a crack element, as shown in Fig. D1.

This procedure uses compatibility and equilibrium requirements, and interested readers could refer to the authors' other publications [45,61] for further details. The probabilistic model developed by Sajedi & Huang [13] is implemented to estimate the average bond strength, τ_m, that is a function of corrosion for intact and corroded specimens as:

$$ln\left(\frac{\tau_m}{\sqrt{f_c'}}\right) = \theta_0 + \theta_1 \cdot exp(\widetilde{\theta}_1 \cdot Q) \cdot \frac{c}{d_{b0}} \cdot \frac{\mu + R_r}{1 - \mu R_r} \cdot \gamma + \theta_2 \cdot exp(\widetilde{\theta}_2 \cdot Q) \cdot \frac{b_e}{d_{b0}} \cdot \frac{\mu + R_r}{1 - \mu R_r} \cdot \gamma + \theta_3 \cdot \frac{1}{\sqrt{f_c'}} \cdot \frac{A_{st} f_{y,st}}{s d_{b0}} + \sigma\varepsilon \quad \text{(D2)}$$

where the predicted coefficients are: $\theta_0 = -0.90$, $\theta_1 = 0.48$, $\theta_2 = 0.12$, $\theta_3 = 0.024$, $\theta_1 = -0.08$, and $\theta_2 = -0.148$; $\mu = 0.45$ [62] is the rebar friction coefficient; $R_r = 0.1$ [63] is the relative lug area of the intact bar; b_e is the effective beam width (mm) ($3c \le b_e \le 9c$); $\gamma = [8 \cdot d_{b0}/(l_d \text{ or } l_s)]^{0.5}$ (≤ 1) is a reduction factor to long development length (l_d) or splice length (l_s); A_{st} is the area of two legs of the transverse reinforcement in the cross-section (mm^2); s = transverse reinforcement spacing (mm); and $\sigma\varepsilon$ is the model error where $\sigma = 0.169$ and ε = standard normal random variable [13].

References

[1] Huang Q, Gardoni P, Hurlebaus S. Probabilistic seismic demand models and fragility estimates for reinforced concrete highway bridges with one single-column bent. J Eng Mech 2010. https://doi.org/10.1061/(ASCE)EM.1943-7889.0000186.

[2] Dehghani Nariman L, et al. A Markovian approach to infrastructure life-cycle analysis: Modeling the interplay of hazard effects and recovery. Earthquake Eng Struct Dyn 2020. https://doi.org/10.1002/eqe.3359.

[3] Zaker Esteghamati M, Banazadeh M, Huang Q. The effect of design drift limit on the seismic performance of RC dual high-rise buildings. Struct Des Tall Spec Build 2018. https://doi.org/10.1002/tal.1464.

[4] Hariri-Ardebili MA, Saouma VE. Seismic fragility analysis of concrete dams: A state-of-the-art review. Eng Struct 2016. https://doi.org/10.1016/j.engstruct.2016.09.034.

[5] Kivell A, Palermo A, Scott A. Effects of bond deterioration due to corrosion in reinforced concrete. Ninth Pacific Conf Eathquake Eng Earthq Resilient Soc 2011.

[6] Almusallam AA, Al-Gahtani AS, Aziz AR. Rasheeduzzafar, Effect of reinforcement corrosion on bond strength. Constr Build Mater 1996. https://doi.org/10.1016/0950-0618(95)00077-1.

[7] Soraghi A, Huang Q, Hauff DAJ. Probabilistic Model for Rebar-Concrete Bond Failure Mode Prediction Considering Corrosion. Am Soc Civ Eng (ASCE) 2019: 362–72. https://doi.org/10.1061/9780784482247.033.

[8] Wang H. An analytical study of bond strength associated with splitting of concrete cover. Eng Struct 2009;31:968–75. https://doi.org/10.1016/j.engstruct.2008.12.008.

[9] Harajli MH. Comparison of bond strength of steel bars in normal- and high-strength concrete. J Mater Civ Eng 2004. https://doi.org/10.1061/(ASCE)0899-1561(2004)16:4(365).

[10] Stanish K, Hooton RD, Pantazopoulou SJ. Corrosion effects on bond strength in reinforced concrete. ACI Struct J 1999;96:915–21. https://doi.org/10.14359/765.

[11] Fu X, Chung DDL. Effect of corrosion on the bond between concrete and steel rebar. Cem Concr Res 1997;27:1811–5. https://doi.org/10.1016/S0008-8846(97)00172-5.

[12] Hussain S, Al-Musallam A, Al-Gahtani A. Factors affecting threshold chloride for reinforcement corrosion in concrete. Cem Concr 1995:1543–55.

[13] Sajedi S, Huang Q. Probabilistic prediction model for average bond strength at steel-concrete interface considering corrosion effect. Eng Struct 2015;99:120–31. https://doi.org/10.1016/j.engstruct.2015.04.036.

[14] ACI. Report on bond of steel reinforcing bars under cyclic loads; 2012.

[15] fib, fib Model Code for Concrete Structures 2010. Wiley-VCH Verlag GmbH & Co. KGaA, Weinheim, Germany; 2013. https://doi.org/10.1002/9783433604090.

[16] Cucchiara C, La Mendola L, Papia M. Effectiveness of stirrups and steel fibres as shear reinforcement. Cem Concr Compos 2004. https://doi.org/10.1016/j.cemconcomp.2003.07.001.

[17] Hanjari KZ, Coronelli D, Lundgren K. Bond capacity of severely corroded bars with corroded stirrups. Mag Concr Res 2011. https://doi.org/10.1680/macr.10.00200.

[18] Harajli MH, Hamad BS, Rteil AA. Effect of confinement of bond strength between steel bars and concrete. ACI Struct J 2004;101:595–603. https://doi.org/10.14359/13381.

[19] El Maaddawy T, Topper T. Long-Term Performance of Corrosion-Damaged Reinforced Concrete Beams; 2005. https://www.researchgate.net/publication/256484201 [accessed May 5, 2020].

[20] Orangun CO, Jirsa JO, Breen JE. Reevaluation of test data on development length and splices. J Am Concr Inst 1977;74:114–22. https://doi.org/10.14359/10993.

[21] Darwin D, Graham EK. Effect of deformation height and spacing on bond strength of reinforcing bars. ACI Mater J 1993;90:646–57. https://doi.org/10.14359/4459.

[22] Yalciner H, Eren O, Sensoy S. An experimental study on the bond strength between reinforcement bars and concrete as a function of concrete cover, strength and corrosion level. Cem Concr Res 2012;42:643–55. https://doi.org/10.1016/j.cemconres.2012.01.003.

[23] Abosrra L, Ashour AF, Youseffi M. Corrosion of steel reinforcement in concrete of different compressive strengths. Constr Build Mater 2011. https://doi.org/10.1016/j.conbuildmat.2011.04.023.

[24] Ahmed SFU, Maalej M, Mihashi H. Cover cracking of reinforced concrete beams due to corrosion of steel. ACI Mater J 2007;104:153–61. https://doi.org/10.14359/18578.

[25] ACI Committee 308, Guide to Curing Concrete, Am. Concr. Institute; 2001. p. 1–31.

[26] Fang C, Gylltoft K, Lundgren K, Plos M. Effect of corrosion on bond in reinforced concrete under cyclic loading. Cem Concr Res 2006;36:548–55. https://doi.org/10.1016/j.cemconres.2005.11.019.

[27] Bandelt MJ, Billington SL. Bond behavior of steel reinforcement in high-performance fiber-reinforced cementitious composite flexural members. Mater Struct Constr 2016. https://doi.org/10.1617/s11527-014-0475-4.

[28] ASTM A944-10. Standard Test Method for Comparing Bond Strength of Steel Reinforcing Bars to Concrete Using Beam-end Specimens. ASTM Int.; 2015. https://doi.org/10.1520/A0944-10R15.2.

[29] ACI. Development of Straight Reinforcing Bars in Tension. ACI 408R-03; 2003.

[30] Harrington P. Machine Learn Act 2012. https://doi.org/10.1007/s10994-011-5249-4.

[31] Chang M, Maguire M, Sun Y. Stochastic modeling of bridge deterioration using classification tree and logistic regression. J Infrastruct Syst 2019. https://doi.org/10.1061/(ASCE)IS.1943-555X.0000466.

[32] Tibshirani R. Journal of the Royal Statistical Society. Series B (Methodological), J R Stat Soc Ser B 1996;58:267–88.

[33] Zamanian Soroush, et al. Significant variables affecting the performance of concrete panels impacted by wind-borne projectiles: A global sensitivity analysis. Int J Impact Eng 2020;144:103650. https://doi.org/10.1016/j.ijimpeng.2020.103650.

[34] Lindsey C, Sheather S. Variable selection in linear regression. Stata J 2010;10:650–69. https://doi.org/10.1177/1536867x1101000407.

[35] Harajli MH. Bond Stress-Slip Model for Steel Bars in Unconfined or Steel, FRC, or FRP Confined Concrete under Cyclic Loading. J Struct Eng 2009. https://doi.org/10.1061/(asce)0733-9445(2009)135:5(509).

[36] Wu YF, Zhao XM. Unified bond stress-slip model for reinforced concrete. J Struct Eng (United States) 2013. https://doi.org/10.1061/(ASCE)ST.1943-541X.0000747.

[37] Lin H, Zhao Y, Yang JQ, Feng P, Ozbolt J, Ye H. Effects of the corrosion of main bar and stirrups on the bond behavior of reinforcing steel bar. Constr Build Mater 2019. https://doi.org/10.1016/j.conbuildmat.2019.07.156.

[38] Lin H, Zhao Y, Ozbolt J, Feng P, Jiang C, Eligehausen R. Analytical model for the bond stress-slip relationship of deformed bars in normal strength concrete. Constr Build Mater 2019. https://doi.org/10.1016/j.conbuildmat.2018.11.258.

[39] Lin H, Zhao Y, Ožbolt J, Reinhardt HW. Bond strength evaluation of corroded steel bars via the surface crack width induced by reinforcement corrosion. Eng Struct 2017. https://doi.org/10.1016/j.engstruct.2017.08.051.

[40] Rodriguez J, Ortega LM, Casal J. Corrosion of reinforcing bars and service life of reinforced concrete structures-corrosion and bond deterioration. Int Conf Concr Across Borders Odense, Denmark 1994.

[41] Castel A, François R, Arliguie G. Mechanical behaviour of corroded reinforced concrete beams - Part 1: experimental study of corroded beams. Mater Struct Constr 2000;33:539–44. https://doi.org/10.1007/bf02480533.

[42] Champiri MD, Hossein Mousavizadegan S, Moodi F. A decision support system for diagnosis of distress cause and repair in marine concrete structures. Comput Concr 2012;9:99–118.

[43] Abdel-Kareem AH. Shear strengthening of reinforced concrete beams with rectangular web openings by FRP Composites. Adv Concr Constr 2014;2:281–300. https://doi.org/10.12989/acc.2014.2.4.281.

[44] ACI Committee 318. Building Code Requirements for Structural Concrete; 2014.

[45] Sajedi S, Huang Q. Load-deflection behavior prediction of intact and corroded RC bridge beams with or without lap splices considering bond stress-slip effect. J Bridg Eng 2017. https://doi.org/10.1061/(ASCE)BE.1943-5592.0000981.

[46] Bamonte PF, Gambarova PG. High-Bond Bars in NSC and HPC: Study on Size Effect and on the Local Bond Stress-Slip Law. J Struct Eng 2007. https://doi.org/10.1061/(asce)0733-9445(2007)133:2(225).
[47] Lin H, Zhao Y, Ožbolt J. The bond behavior between concrete and corroded steel bar under repeated loading. Eng Struct 2017. https://doi.org/10.1016/j.engstruct.2017.02.067.
[48] Wu Z, Zhang X, Zheng J, Hu Y, Li Q. Bond Behavior of Plain Round Bars Embedded in Concrete Subjected to Biaxial Lateral Tensile-Compressive Stresses. J Struct Eng 2014. https://doi.org/10.1061/(asce)st.1943-541x.0000872.
[49] Coronelli D, Gambarova P. Structural assessment of corroded reinforced concrete beams: Modeling guidelines. J Struct Eng 2004;130:1214–24. https://doi.org/10.1061/(ASCE)0733-9445(2004)130:8(1214).
[50] Lundgren K. Bond between ribbed bars and concrete. Part 2: The effect of corrosion. Mag Concr Res 2005. https://doi.org/10.1680/macr.2005.57.7.383.
[51] Zhang Y, Bicici E, Sezen H, Zheng S. Reinforcement slip model considering corrosion effects. Constr Build Mater 2020;235. https://doi.org/10.1016/j.conbuildmat.2019.117348.
[52] Nakamura H, Srisoros W, Yashiro R, Kunieda M. Time-dependent structural analysis considering mass transfer to evaluate deterioration process of RC structures. J Adv Concr Technol 2006. https://doi.org/10.3151/jact.4.147.
[53] Sajedi S, Huang Q, Gandomi AH, Kiani B. Reliability-Based Multiobjective Design Optimization of Reinforced Concrete Bridges Considering Corrosion Effect. ASCE-ASME J Risk Uncertain Eng Syst Part A Civ Eng 2017;3. https://doi.org/10.1061/AJRUA6.0000896.
[54] Lu R, Luo Y, Conte JP. Reliability evaluation of reinforced concrete beams. Struct Saf 1994;14:277–98. https://doi.org/10.1016/0167-4730(94)90016-7.
[55] Huang Q, Gardoni P, Hurlebaus S. Adaptive Reliability Analysis of Reinforced Concrete Bridges Subject to Seismic Loading Using Nondestructive Testing. ASCE-ASME J Risk Uncertain Eng Syst Part A Civ Eng 2015. https://doi.org/10.1061/ajrua6.0000835.
[56] Karbassi A, Mohebi B, Rezaee S, Lestuzzi P. Damage prediction for regular reinforced concrete buildings using the decision tree algorithm. Comput Struct 2014. https://doi.org/10.1016/j.compstruc.2013.10.006.
[57] Fisher RA. The use of multiple measurements in taxonomic problems. Ann Eugen 1936;7:179–88. https://doi.org/10.1111/j.1469-1809.1936.tb02137.x.
[58] Friedman JH. Regularized discriminant analysis. J Am Stat Assoc 1989. https://doi.org/10.1080/01621459.1989.10478752.
[59] James G, Witten D, Hastie T, Tibshirani R. An Introduction to Statiscal Learning with Applications in R; 2013. https://doi.org/10.1016/j.peva.2007.06.006.
[60] Zhang J, Ma G, Huang Y, Sun J, Aslani F, Nener B. Modelling uniaxial compressive strength of lightweight self-compacting concrete using random forest regression. Constr Build Mater 2019. https://doi.org/10.1016/j.conbuildmat.2019.03.189.
[61] El Maaddawy T, Soudki K, Topper T. Analytical model to predict nonlinear flexural behavior of corroded reinforced concrete beams. ACI Struct J 2005. https://doi.org/10.14359/14559.
[62] Choi OC, Lee WS. Interfacial bond analysis of deformed bars to concrete. ACI Struct J 2002;99:750–6. https://doi.org/10.14359/12339.
[63] Wang X, Liu X. Modeling bond strength of corroded reinforcement without stirrups. Cem Concr Res 2004;34:1331–9. https://doi.org/10.1016/j.cemconres.2003.12.028.